Thesis for the Degree of Doctor of Physics

The first principles study on magnetism of nano-material defect

by

Jeonghwa Yang

Department of Physics

The Graduate School

Pukyong National University

February 2013

The first principles study on magnetism of nano-material defect

(결함을 가진 나노물질의 자성에 대한 제일원리 연구)

Advisor: Prof. Jisang Hong

by

Jeonghwa Yang

A thesis submitted in partial fulfillment of the requirements
for the degree of Doctor of Physics

in Department of Physics, The Graduate School,
Pukyong National University

February 2013

The first principles study on magnetism of nano-material defect

A dissertation

by

Jeonghwa Yang

Approved by:

Chanyong Hwang (Chairman)

Jisang Hong (Member)

Byung Chun Choi (Member)

Sung Heum Park (Member)

Jae-Won Jang (Member)

February 22, 2013

The first principles study on magnetism of nano-material defect

Jeonghwa Yang

Department of Physics, The Graduate School,
Pukyong National University

Abstract

We have explored the magnetic properties of hexagonal 2p systems, hexagonal boron nitride (h-BN) and graphene using the full potential linearized augmented plane wave (FLAPW) method.

First of all, we have explored the origin of magnetism based on the hexagonal boron nitride (h-BN) systems. It has been observed that the N vacancy defect has no influence on the magnetic property of *h*-BN, whereas the B vacancy defect induced spin polarization in the nearest three N atoms. Both B and N adatom defect systems preserve close to semiconducting feature with a finite band gap. We have found that the Density of state (DOS) and the X-ray magnetic circular dichroism (XMCD) spectral shapes are strongly dependent on the defect type. Also, we have investigated the magnetic properties of a hexagonal boron nitride (h-BN) monolayer induced by a 0.5 monolayer of oxygen (O) and fluorine (F) adlayers. It has been observed that the F and O adlayers are adsorbed on the boron top site in the most stable structure. We find that both systems display ferromagnetic ground states. In F/BN, the calculated magnetic moments of F and N atoms are 0.18 and $0.44\,\mu_B$. Also, the band structure of F/BN is very close to half-metallic. In O/BN, the

calculated magnetic moments of O and N atoms are 0.91 and $0.4\mu_B$. The band structure shows a metallic state. Interestingly, it has been found that the O/BN may show a ferromagnetic ground state far beyond room temperature.

Second, we report the theoretical results that the carrier induced switching of magnetic interaction between two magnetic layers in Co(111)/Graphene/Ni(111) (Co/Gr/Ni) is predicted. The Co/Gr/Ni shows an antiferromagnetic (AFM) ground state when there are no external carriers. The antiferromagnetic interaction is still observed for hole carriers. However, the magnetic exchange interaction between Ni and Co layers can be manipulated in such a way as to change an AFM to a ferromagnetic (FM) state by injecting external electrons. Overall, we propose that a potential spin switching by external carriers or electric field can be realized in Co/Gr/Ni. Besides, the calculated DOS feature indicates that the Co/Gr/Ni system may manifest quite different transport properties when a bias voltage is applied. For instance, the current parallel to the film surface can be completely spin-polarized from minority spin-electrons. In contrast, the current perpendicular to the film surface will be positively spin polarized from majority spin- electrons.

Contents

List of figures

List of tables

1. Introduction

It is a common belief that a 3d transition metal element is an essential entity for displaying a magnetic state in any materials [1]. However, recently, many studies have reported that the magnetic state can be observed in the material without conventional magnetic elements, such as Mn, Fe, Co, and Ni, so called "d^0 magnetism" Specifically, the carbon based hexagonal graphene system among the d^0 magnetism is of particular interest because the graphene system shows many extraordinary physical properties and the magnetic graphene may have many advantages for spintronics applications as compared with other metallic materials or dilute magnetic semiconductor.

One of the most interesting aspects of the graphene system is that its low-energy excitations are massless, chiral, Dirac fermions. In graphene, the chemical potential crosses exactly the Dirac point. This particular dispersion, that is only valid at low energies, mimics the physics of quantum electrodynamics (QED) for massless fermions except for the fact that in graphene the Dirac fermions move with a speed v_F, which is 300 times smaller than the speed of light c. Possibly even more importantly, the recent experimental demonstrations of magnetism in a pure carbon system have ignited speculation that carbon could offer the tantalizing prospect of a zero-gap, high-temperature, ferromagnetic semiconductor [2-4]. Likewise, many

studies have focused on the electric properties of graphene systems since the ideal graphene is non-magnetic. It will be of particular interest if the physical property of graphene layer can be utilized for spintronics purposes.

Another interesting hexagonal system like graphene is a boron nitride film. As is well known, the hexagonal boron nitride and graphene systems are isoelectronic and the lattice constants are also very close to each other. Due to these similarities, the hexagonal boron nitride has also attracted extensive research interests for potential spintronics application purposes. However, despite the isoelectronic with carbon based material, it is found that the h-BN systems show a wide band gap semiconducting feature [14]. On the other hand, like in the graphene system, it will be of interest to explore the magnetic property of the h-BN system for potential spintronics application as well. So, We have focused on magnetic properties in the h-BN systems. First, we will calculate the influence of vacancy defect or adatom defect on the magnetic property of the h-BN monolayer. Also, we will find any indication whether the magnetic property of the h-BN monolayer depends on the defect type. Second, we have investigated the magnetic properties of a hexagonal boron nitride (h-BN) monolayer induced by a 0.5 monolayer of oxygen (O) and fluorine (F). We should calculate the most stable structure, magnetic properties and band structure.

Regarding the magnetism in graphene, it has been predicted by various theoretical studies about the vacancy or adatom defect. However, it is rather difficult to control the magnetism arising from the defects since the magnetic state will be affected by various factors such as relative distance between defects, defects concentration, or adsorption sites [5–8]. To study magnetic graphene many researchers have investigated multilayer systems such as graphene/Ni, graphene/Co. These systems have structual stability because lattice mismatch between Ni(111) and graphene layer or Co(111) and graphene is quite small [9-13]. Due to these reason, many researchers have investigated multilayer system but they have not obtain useful information for spintronics purpose. For this reason, we will explore the fundamental magnetic property of trilayer system including graphene material. Based on this result, we will investigate the influence of external carrier type and concentration on the magnetic exchange coupling between two magnetic layers. We expect that our theoretical study will provide useful information for potential spintronics purpose.

2. Methodologies

2.1 Density functional theory (DFT)

The density functional theory originated from the statistical theory of atoms proposed independently by Tomas [14],Fermi [15],Dirac [16]. The theory was formally completed by Hohenberg and Kohn(HK) [17], and Kohn and Sham(KS) [18]. Density functional theory is known as important means for researching structure of electron theoretically and provides very powerful ways to treat problem in many body system as a form of one particle system.

2.1.1. Hohenberg - Kohn theorem

The first-principles calculation is based on the density functional theory. Early DFT was found in Thomas-Fermi theory [14,15] which represented energy in ground state with only equation of density. Strictly speaking the basis of DFT was Hohenberg-Kohn theorem [17].

This theorem supposes that the characteristic of ground state in system of particle could be presented with only density in that state. Therefore exact calculation of density in ground state is proved to be possible from the principle in which only density would be included. Hamiltonian in many body systems could be written like as follow.

$$H = \hat{T} + \hat{V} + \hat{U} \tag{1}$$

Here $\hat{T}$, $\hat{V}$ and $\hat{U}$ represents Kinetic energy, external potential and Coulomb energy respectively. Given only external potential to system

we could find out total Hamiltonian. If system would be limited in non-degenerated systems corresponding eigenstate and density could be calculated with Schrodinger function

$$\hat{H}|\Psi = E|\Psi> \tag{2}$$

So function like $\hat{V} \rightarrow \Psi \rightarrow \rho(\vec{r})$ exists. Hohenberg-Kohn theorem supposes that in ground state function is one to one and invertible.
In other words external potential would be decided by electron density. This suggests various form of energy function

$$\begin{aligned} E_\nu[\rho] &= <\Psi[\rho]|\hat{H}|\Psi[\rho]> \\ &= <\Psi[\rho]|\hat{T}+\hat{U}|\Psi[\rho]> + <\Psi[\rho]|\hat{V}|\Psi[\rho]> \end{aligned} \tag{3}$$

$$E_\nu[\rho] = F_{HK}[\rho] + \int d\vec{r} v(\vec{r})\rho(\vec{r}) \tag{4}$$

and Hohenberg-Kohn function, $F_{HK}[\rho]$, would not be affected by external potential $\nu(\vec{r})$. Second equation of Hohenberg-Kohn theorem would be proved to be like in any density ρ.

$$E_0 \leq E_v[\rho] \tag{5}$$

Here E_0 represents energy in ground state and would be stable only if $\rho = \rho_0$. ρ_0 represents density of ground state. So exact density of ground state could be decided with minimum value of $E_\nu[\rho]$.

2.1.2. Kohn-Sham Equation

Hohenberg & Kohn, and Kohn & Sham have suggested that total energy in system like solid or surface is dependent on only charge density in ground state [17,18].

$$E = E[\rho] \tag{6}$$

The idea of using charge density in quantum mechanics theory to substantial had been started long time ago but only after decades that had been started to be adapted in molecule system with development of Hartree-Fock approximation and further in system of solid state. Slater used electron gas for calculation of solid state using Hartree-Fock approximation. This method was X_α and has contributed for developing more sophisticated method of calculating electron structure. Charge density is scalar function defined each point $\vec{r}$ in real space.

$$\rho = \rho(\vec{r}) \tag{7}$$

Charge density and total energy would be dependent on a kind and location of core atom like

$$E = E[\rho(\vec{r}), \overrightarrow{R_\alpha}] \tag{8}$$

In this $\overrightarrow{R_\alpha}$ is set of location of all atom α in any system considered. (equation 8) is an important one for understanding electron structure of substance and dynamic characteristic in atom system and with this equation we could predict equilibrium of particles on the surface and cohesive energy of solid. And in this equation if total energy would be differentiate with the core of each atom we could get the force acting in that atom and find out stable structure of the system, therefore we could study dynamic procedure like diffusion or reaction of particles on the surface.

In DFT total energy (equation 6) can be divided into kinetic energy, Coulomb energy and exchange-correlation like (equation 6).

$$E = T_0 + U + E_{xc} \tag{9}$$

Coulomb energy U can be calculated with traditional method and this can be divided into attraction between electron and core, repulsive force between electron and that among cores again.

$$U = U_{en} + U_{ee} + U_{nn} \tag{10}$$

U_{en}, U_{ee},and U_{nn} can be define is

$$U_{en} = -e^2 \sum_{\alpha} Z_\alpha \int \frac{\rho(\vec{r})}{|\vec{r} - \vec{R}|} d\vec{r} \tag{11}$$

$$U_{ee} = e^2 \iint \frac{\rho(\vec{r})\rho(\vec{r'})}{|\vec{r} - \vec{r'}|} d\vec{r} d\vec{r'} \tag{12}$$

$$U_{nn} = e^2 \sum_{\alpha\alpha'}^{\alpha} \frac{Z_\alpha Z_{\alpha'}}{|\overrightarrow{R_\alpha} - \overrightarrow{R_{\alpha'}}|} \tag{13}$$

Kinetic energy T_o is more complicate. According to DFT actual electron of system could be changed into effective electron with the same amount of electric charge, mass and contribution of density. Real electron is affected by all other electron but effective electron moves as particles not related to effective potential, so T_o can be represented with the sum of kinetic energy of all effective electron.

If effective electron would be stated with wave function ψ_i of single particle, kinetic energy of all effective electron in the system could be represented with

$$T_o = \sum_i n_i \int \psi_i^*(\vec{r}) \left[\frac{-\hbar^2}{2m} \nabla^2 \right] \psi_i(\vec{r}) d\vec{r} \tag{14}$$

Equation 14 is the sum of expected value to kinetic energy of a particle and n_i is defined as the number of electron in the state of i.

E_{xc}(exchange-correlation energy), last term of (equation 9) is included energy by contribution of all extra complicate electron

In this the most important contribution is the term of exchange term. An electron is fermion, so according to Pauli's exclusion principle an electron with the same spin is not impossible to exist on the same orbit that is why mean Coulomb repulsion which would act on electron would be decreased and the energy generated in that moment called as "exchange energy". If each electron would be considered to be surrounded with positive exchange hole, total electric charge summed by all exchange hole could be +e . According to definition additional many body problem among electrons with opposite spin would be called as "correlation energy". Kinetic energy and Coulomb energy have opposite sign and almost same amount but correlation energy is about 10% of Coulomb energy. Correlation energy is much smaller than exchange energy but plays an important role in conclusion of length and strength of atomic combination.

Binding energy of solid and atoms on the surface is much smaller than total energy, so it ranges in about 1~8 eV and energy which would change position of atoms on the surface is also very small.

Most important Hohenberg-Kohn-Sham theorem in DFT represents that total energy under density of ground state would have minimum value like (equation 15).

$$\frac{\partial \vec{E}[\rho]}{\partial \rho}|_{\rho=\rho_o} = 0 \qquad (15)$$

If wave function of single particle would be $\psi_i(\vec{r})$, electron density, $\rho(\vec{r})$ could be stated as (equation 16).

$$\psi_i(\vec{r}) = \sum_i n_i |\psi(\vec{r})|^2 \tag{16}$$

As (equation 14) for kinetic energy n_i is defined as the occupation number in the eigenstate in which that would be represented with wave function of single particle, $\psi_i(\vec{r})$.

In (equation 14~16) wave function of single particle has been used and variation in this wave function corresponds with that of electron density, so the condition of single particle wave function under ground state density can be induced from the condition of calculus of variation of (equation 15). This equation is called as "**Kohn-Sham equation**"

$$\left[\frac{\overrightarrow{\hbar^2}}{2m}\nabla^2 + V_{eff}(\vec{r})\right]\psi_i(\vec{r}) = \epsilon_i\psi_i(\vec{r}) \tag{17}$$

In this $V_{eff}(\vec{r})$ is represented with (equation 18).

$$V_{eff}(\vec{r}) = V_c(\vec{r}) + \mu_{xc}[\rho(\vec{r})] \tag{18}$$

The electron density which corresponds to this wave function would be density in ground state which would make total energy minimum. The solution of **Kohn-Sham** equation forms orthonormalized set of

(equation 19).

$$\int \psi_i^*(\vec{r})\psi_j(\vec{r})d\vec{r} = \delta_{ij} \tag{19}$$

Because in (equation 9) total energy is divided into 3 terms Kohn-Sham equation has also 3 terms. Kinetic energy is second order differential operator of Shrodinger equation of single particle and is not related to the system. In contrast $V_c(\vec{r})$, operator of Coulomb potential, and μ_{xc}, operator of exchange correlation potential, are dependent on contribution of electron in considered system. $V_c(\vec{r})$, Coulomb potential, on point $\vec{r}$ are generated from charge of core and electron in the system and calculated immediately in real space like (equation 20).

$$V_c(\vec{r}) = -e^2 \sum_{\alpha} \frac{Z_\alpha}{|\vec{r} - \vec{R_\alpha}|} + e^2 \int \frac{\rho\vec{r'}}{|\vec{r} - \vec{r'}|} d\vec{r'} \tag{20}$$

In condensed system for calculating Coulomb potential we should solve Poisson equation of (equation 21).

$$\nabla^2 V_c(\vec{r}) = -4\pi e^2 q(\vec{r}) \tag{21}$$

Exchange correlation potential is related to exchange correlation

energy (or exchange correlation potential).

$$\mu_{xc} = \frac{\partial E_{xc}[\rho]}{\partial \rho} \tag{22}$$

In actual calculation exchange correlation energy (or exchange correlation potential) is not well known and it could be calculated with approximation method like LDA or GGA etc.

2.1.3. Local density approximation (LDA) and local spin density approximation (LSDA)

All complicate phenomena of physics in interaction system could be solved by calculating standardized equation of $E_{xc}[\rho]$. It is natural to use characteristics of uniform electromagnetic bodyinteracted on density of slow variation. In other words put exchange correlation energy density as ε_{xc} it would be dependent on only $\rho(\vec{r})$, local density.

$$E_{xc}[\rho] = \int \rho(\vec{r}) \epsilon_{xc}[\rho(\vec{r})] d\vec{r} \tag{23}$$

Exchange correlation energy is dependent on only local density of electron around of each $d\vec{r}$, volume element. This method of approximation is called as LDA. LDA has two hypothesis, first the effect of exchange correlation would be domain only around the point

and second the effect of that would not be dependent on variation of electron density around. Therefore in volume element it could be treated as the same density of electron. The approximation like this would be correspondent in the system of metal but should be used with precaution in the system in which variation of electron density would be great.

We have make an effort to understand a system of electron with uniform density and research characteristics. Especially exchange correlation energy per electron of uniform electron gas has been calculated with various method of approximation like many body perturbation theory and Monte Carlo method. In actual calculation it would be represented analytic function of electron density and in expression of term of exchange correlation there are various analytic forms with different coefficient. For example in the system in which spin polarization would not be accounted for, the term of local density exchange by Kohn & Sham would be

$$\epsilon_x = -\frac{3}{2}\left(\frac{3}{\pi}\rho\right)^{\frac{1}{3}}, \mu_x = -2\left(\frac{3}{\pi}\rho\right)^{\frac{1}{3}} \tag{24}$$

and the term of correlation by Hedin and Lundqvist would be

$$\epsilon_c(\rho) = -C\frac{e^2}{a_0}\left[(1+x^3)\ln\left(1+\frac{1}{x}\right)+\frac{x}{3}-x^2-\frac{1}{3}\right] \tag{25}$$

here, $C=0.0225$, a_0 is Bohr radius and

$$x = \frac{r_s}{21a_0} \tag{26}$$

$$r_s = \left[\frac{3}{4\pi\rho}\right]^{\frac{1}{3}} \tag{27}$$

exchange correlation energy ϵ_{xc} and exchange correlation potential, μ_{xc} would be

$$\epsilon_c(\rho) = \epsilon_x + \epsilon_c \ , \ \mu_{xc} = \frac{\partial \rho \epsilon_{xc}}{\partial} \tag{28}$$

In the case of transition metal with magnetic force on the surface the method in which spin polarization would be accounted for due to non coupled electron should be used. The system like this LSDA will be used because the number of "majority spin" and "minority spin" would be different [20,21]. In LSDFT $\rho(\vec{r})$, electron density, and $\sigma(\vec{r})$, spin density, will be used. Density of spin density $\sigma(\vec{r})$ would be defined as the difference between majority spin and minority spin, in other words as (equation 29).

$$\sigma(\vec{r}) = \rho_{\uparrow}(\vec{r}) - \rho_{\downarrow}(\vec{r}) \tag{29}$$

and density of electron would be

$$\rho(\vec{r}) = \rho_{\uparrow}(\vec{r}) + \rho_{\downarrow}(\vec{r}) \tag{30}$$

In LSDA theory effective potential of (equation 18) would be dependent on the spin because exchange correlation potential by majority spin and minority spin is generally different. So Kohn-Sham equation in which spin polarization would be accounted for would be

$$\left[\frac{-\hbar^2}{2m_e}\nabla^2 + V_{eff}(\vec{r})\right]\psi_i(\vec{r}) = \epsilon_i\psi_i(\vec{r}) \tag{31}$$

Here, V_{eff} is

$$V_{eff}(\vec{r}) = V_c(\vec{r}) + \mu_{xc}[\rho(\vec{r})] \tag{32}$$

Hamiltonian is stated as follow

$$H = \hat{T} + \hat{V} + \hat{U} \tag{33}$$

and here in a system in which magnetic field is $b(\vec{r})$ and magnetization density is $m(\vec{r})$ it is

$$\hat{V} = \int [v(\vec{r})\rho(\vec{r}) - b(\vec{r})m(\vec{r})]d\vec{r} \tag{34}$$

and here it is

$$\rho(\vec{r}) = \psi_\alpha{}^*(\vec{r})\psi_\alpha(\vec{r}) \tag{35}$$

and

$$m(\vec{r}) = -\mu_0 \sum_{\alpha,\beta} \sigma_{\alpha,\beta}\, \psi_\alpha{}^*(\vec{r})\psi_\beta(\vec{r}) \tag{36}$$

In this α is spin index and, μ_0 is Bohr magneton. And $\sigma_{\alpha,\beta}$ is Pauli spin matrix vector. If it would be defined with

$$\omega(\vec{r}) \equiv \{v(\vec{r}), b(\vec{r})\} \tag{37}$$

$$v(\vec{r}) \equiv \{\rho(\vec{r}), m(\vec{r})\} \tag{38}$$

, v(r) could only decide ω(r) the same method about non magnetic system. Proper energy function would be as follow

$$E_\omega[V(\vec{r})] = \int \{v(\vec{r})\rho(\vec{r}) - b(\vec{r})m(\vec{r})\}d\vec{r} + \frac{1}{2}\int \frac{\rho(\vec{r})\rho(\vec{r'})}{|\vec{r}-\vec{r'}|}d\vec{r}d\vec{r'} + G[v(\vec{r})] \quad (39)$$

In this $G[\nu(\vec{r})]$ is general function. $G[\nu(\vec{r})]$ would not be changed under independent spin on $\vec{r}$ in field of magnetization density $m(\vec{r})$. In given $\omega(\vec{r})$ function $E_\omega[\nu]$ would be in its minimum to precise $\nu(\vec{r})$. $G[\nu(\vec{r})]$ is divided into kinetic energy and exchange correlation energy which would not interact and if it would be solved it would be as follow

$$G[v] = T_s[v] + E_{xc}[v] \quad (40)$$

$$T_s[v] = \int d\vec{r}\rho(\vec{r})t_s[\mu(\vec{r})] + \Lambda \quad (41)$$

$$E_{xc}[v] = \int d\vec{r}\rho(\vec{r})\varepsilon_{xc}[\mu(\vec{r})] + \Lambda \quad (42)$$

$\nu(\vec{r})$, t_x and ϵ_{xc} of electromagnetic which change slowly would be adapted in the uniform system and omitted term is adjustment of gradient. This is called as LSDA.

Basic calculation to t_s will be

$$t_s(\rho,\zeta)=\frac{3}{10}k_F^2(\rho)\ \frac{(1+\zeta)^{\frac{5}{3}}+(1-\zeta)^{\frac{5}{3}}}{2} \tag{43}$$

$$\zeta(\vec{r})=\frac{\overrightarrow{m}(\vec{r})}{\overline{m}(\vec{r})} \quad ,\overline{m}\equiv-\mu_0\rho(\vec{r}) \tag{44}$$

and here parameter $\zeta(\vec{r})$ would state angle of local magnetization. $\overline{m}$ is maximum magnetization. $k_F(\rho)$ is Fermi momentum of non magnetic electromagnetic body with density ρ. Local exchange and correlation ϵ_{xc} would be approximated with interpolation between the case of paramagnetism($\zeta=0$) and ferromagnetism($\zeta=1$)[7]. Here

$$\epsilon_{xc}(\rho,\zeta)=\epsilon_{xc}^P+f(\zeta)\Delta\epsilon_{xc}(\rho) \tag{45}$$

$$\epsilon_{xc}^P=\epsilon_{xc}(\rho,\zeta=0) \tag{46}$$

$$\Delta\epsilon_{xc}(\rho)\equiv\epsilon_{xc}(\rho,\zeta=1)-\epsilon_{xc}(\rho,\zeta=0)\equiv\epsilon_{xc}^F(\rho)-\epsilon_{xc}^P(\rho) \tag{47}$$

$$f(0)=0 \quad ,f(1)=1 \tag{48}$$

like in non magnetic system, self-consistent equation to electron of spin-up and spin-down as follow from static equation $E_\omega[\nu]$.

(equation 50-51-52) here $\overline{\mu}$ is chemical potential in ground state. Both

$\vec{b}(\vec{r})$ and $\overrightarrow{m}(\vec{r})$ have only one element. In other words $\vec{b}(\vec{r}) = \overrightarrow{b_z}(\vec{r})\hat{k}$ and $\overrightarrow{m}(\vec{r}) = \overrightarrow{m_z}(\vec{r})\hat{k}$.

2.1.4. Generalized gradient approximation(GGA)

L(S)DA would not fit in the system in which electric charge would be localized like transition metal because in this method localized uniform electric charge of electromagnetic body would be used in not uniform system. In L(S)DA combination force of particles and solid has been overestimate and gap of semi-conductor has been underestimate. And in calculation total energy of iron it is suggested that ferromagnetism of bcc would have lower energy. For complement of problems of LDA Generalized gradient approximation has been recently developed[22,23]. Generalized gradient approximation could derive much better result than L(S)DA in not uniform system because electron density in each point in the space and gradient as well in the case of treating exchange correlation function. So, Generalized gradient approximation can be called "non local" potential also. GGA has been complemented by Perdew and Wang and up to now has been complemented continuously[23]. For example

$$E_{GGA} = E_{LDA} + E_x^G + E_c^G \tag{53}$$

and exchange E_x^G term suggested by Becke is

$$E_x^G = b\sum\int \frac{\rho_\sigma x_\sigma^2}{1+6bx_\sigma \sinh^{-1} x_\sigma} d\vec{r} \tag{54}$$

$$x_\rho = \frac{|\nabla\rho|}{\rho_\sigma^{\frac{4}{3}}} \quad , \quad \sigma = \uparrow \text{or} \quad \downarrow \tag{55}$$

and E_c^G by Perdew is

$$E_c^G = \int f(\rho_\uparrow, \rho_\downarrow) e^{g(\rho)|\nabla\rho|} |\nabla\rho|^2 d\vec{r} \tag{56}$$

2.1.5. The Electronic Structure Methods

The quest to solve the Kohn-Sham equation efficiently for periodic solids, solids with surfaces and interfaces, clusters and molecules has lead to a wide spectrum of very successful and efficient electronic structure methods. Treating isolated clusters or molecules, methods based on localized orbitals are frequently selected going hand in hand with the chemical intuition of the system in question. Considering methods applicable to periodic solids, frequently algorithms are chosen where the Bloch boundary condition can be included in the basis set. Guiding principles to develop electronic structure methods are obtained by having a closer look at the mathematical nature of the Schr¨odinger-like Kohn-Sham equation with the kinetic energy operator

$\frac{\hbar^2}{2m}\nabla^2$ and the $1/r$ singularity at the nucleus with the simultaneous necessity to calculate the xc-potential $\mu_{xc}[n](\vec{r})$. and the Hartree potential $V_H[n](\vec{r})$. The planewave basis is obviously a very good choice, as the planewave is diagonalto the Laplace operator $\nabla^2(\triangle)$ appearing in both the kinetic energy operator and the Poisson equation to calculate the Hartree potential, and for a function expanded in planewaves, its power is also completely expressible by a planewave expansion. This property is needed for calculating the charge density from the wave function. Thus, using a planewave basis set, the calculation of the kinetic energy, charge density, and the Hartree potential are obtained by simple algebraic expressions. The calculation of the μ_{xc} can be best performed if the charge density is expressed in real-space. The discrete fast Fourier transformation (FFT) provides a fast algorithm to communicate between both spaces. However, planewave basis sets do not converge at the presence of the $1/r$ singularity. Thus, planewave basis sets can only be used in the context of a pseudopotential approximation to the true potential where the $1/r$ potential has been replaced by an appropriate smooth potential. All-electron methods have to cope with the $1/r$ singularity. Since this singularity cannot be dealt with variationally, one typically works here with basis functions, which are the numerical solution of $(-\nabla^2 + V_{eff} - E_l)\varphi = 0$ of the effective (spherical) potential containing the

$1/r$ singularity, computed in a sphere around the atom at a given energy parameter E_l. These basis functions treat the singularity exactly. The matching of this wavefunction in such a sphere to the rest of the crystal outside the sphere divides the all-electron methods with regard to the eigenvalue dependence of the basis set into two groups: The nonlinear methods as for example the Korringa-Kohn-Rostocker (KKR) method [89] and the APW method, and the linear methods, of which the most commonly used are the linear muffin-tin orbital method (LMTO)[66], the augmented spherical [67] and the APW-based schemes, e.g. FLAPW method [68].

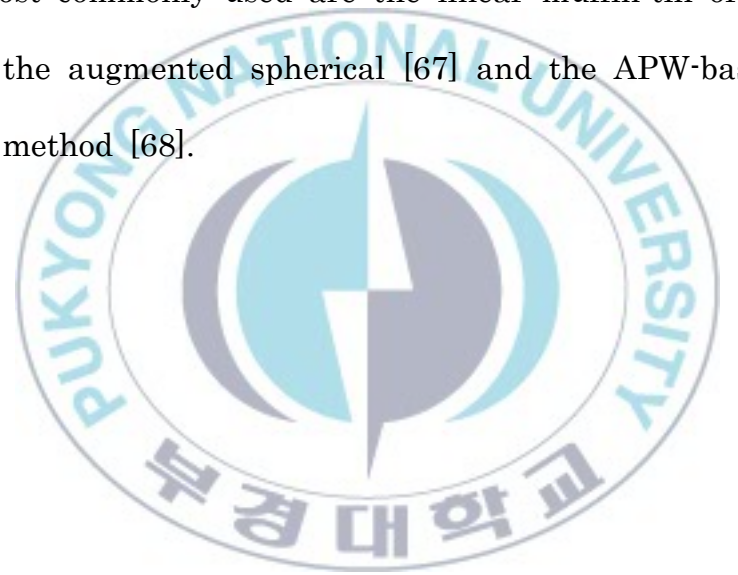

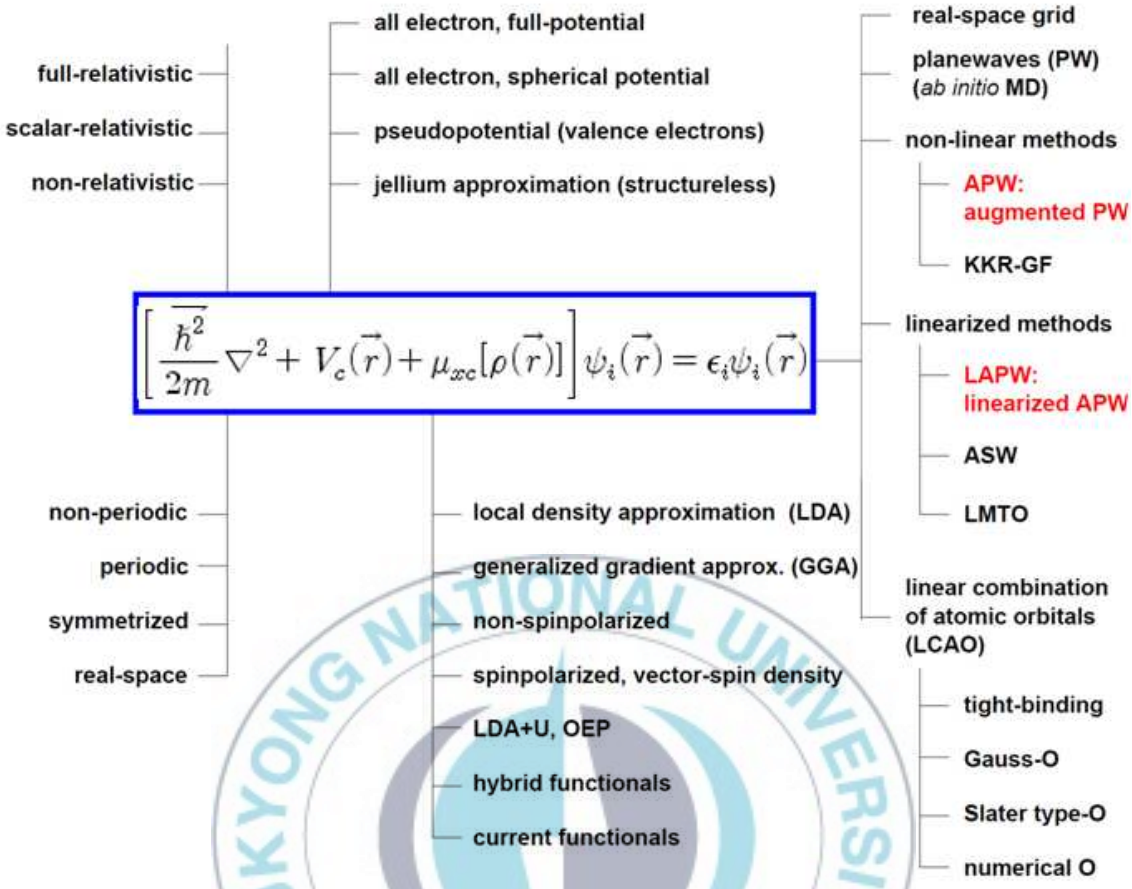

Figure 1. Very rough and schematic overview of electronic structure methods indicating a rich spectrum of methods developed for different purposes, applications, geometries and symmetries, chemical elements and materials requiring different approximations.

3. Method of FLAPW

The most important fact which should be accounted for in calculating electro structure of substance is interaction in the system of particle among electrons. Because complicate interaction in the system of particle among electrons would decide various and subtle property of substance. But generally LSDA by DFT will be used because actually interaction among countless electrons over Avogadro's number would be impossible to be treated directly.

DFT established by Hohenberg and Kohn is based on the theorem in which when energy in ground state in the system of particle would be important DFT of electric charge density and that of ground state. And with LDA a potential on a point could be represented with density of electric charge on that point, so kinetic equation of quantum mechanics in the system of electrons could be represented with equation of single particle like Kohn-Sham equation. Accordingly if you would like to research electron structure you would solve Kohn-Sham equation numerically. For single solution of equation by DFT there are various ways according to method of statement of wave function, electric potential, exchange correlation potential and relativistic consideration of Kohn-Sham equation. Method of FLAPW is known for the most precise calculation of Kohn-Sham equation up to now and it has been widely used for research of various substances. And for calculating property of

surface and interface single slab structure would be used. Single slab divides into 3 area like Muffintin around core, vacuum both ends of thin slab and interstitial and would be calculated in consideration of each area. In this moment wave function in each area shall be developed as basis function according to geometric forms. That is in MT sphere spherical harmonics, in vacuum area linear function and in interstitial area plane wave function would be developed as basis function. Wave function in each area would be linear, in other words wave function should be composed in consideration of first order differentiation function and be continuous on the boundary in each area. Static potential in equation of single particle would be decided by solving Poisson equation with method of pseudocharge designed by Weninert [11]. Exchange correlation potential would be calculated by Least Square Method with use of function form in which density of charge would have been given like Hedin-Lundqvist[6]or Von Varth-Hedin [7]. The system of core of electrons is treated relativistically and valence electron is treated in proportional relativistically in consideration with all relativistic terms except for the term of interaction of spin-orbit. Method of FLAPW could also derive much more precise result because the approximation according to form like spin density and potential etc would never been used. Likewise Method of FLAPW could be stated as the method for exact calculation of various magnetism on the surface and interface and rearrangement

on the surface as well in comparison with other methods[25].

If wave function of single particle $\psi(\vec{k},\vec{r})$ would be developed to reciprocal lattice G, the result would be as follow

$$\psi(\vec{k},\vec{r})\sum_{G} c_{i,k}(G)\phi(\vec{k}+\vec{G},\vec{r}) \tag{57}$$

here each basis function ± is Linear Augmented Plane Wave: LAPW given in following equation.

$$\phi(\vec{k}+\vec{G},\vec{r}) = \Omega^{-1/2} e^{i(k+G)r} \qquad \vec{r}\in institial$$

$$\phi(\vec{K}+\vec{G},\vec{r}) = \sum_{L}[\vec{A_L}(\vec{K}+\vec{G}]\,\vec{U_l}(\vec{E_l},\vec{r}) + \vec{B_l}(\vec{K}+\vec{G})\dot{u}(\vec{E_l},\vec{r})]\,\vec{Y_l}(\hat{r}) \qquad \vec{r}\in MTsphere$$

$$\phi(\vec{K}+\vec{G},\vec{r}) = \sum_{v}[\vec{A_v}(\vec{K}+\vec{G})u_{\vec{K}+\vec{G}}(\vec{E},z) + \vec{B_v}(\vec{K}+\vec{G})\dot{u}_{\vec{K}+\vec{G}}(\vec{E_v},\vec{z})]e^{j(\vec{K}+\vec{G})r} \qquad \vec{r}\in vacuum$$

(58)

element of G is defined from the thickness of thin slab and Ω is the volume of unit cell. Radial function $u_l(E_l,\vec{r})$ is energy E_l regulated in muffin-tin sphere and would be solved with solution of radial Schrodinger equation with spherical effective potential.

$$\frac{1}{\vec{r}}\frac{d^2}{d\vec{r}}(\vec{r}u_l)-\frac{l(l+1)}{\vec{r}^2}u_l+2(\vec{E_l}-\vec{V})u_l=0 \tag{59}$$

$\dot{u}(E_l,\vec{r})$ is a differentiation of energy of u_l and it satisfies form of differentiation of that, so it would be

$$\frac{1}{\vec{r}}\frac{d^2}{d\vec{r}}(\vec{r}\dot{u})-\frac{l(l+1)}{\vec{r}^2}\dot{u}+2(E_l-V)\dot{u}+2u_l=0 \tag{60}$$

And u_{lz} is regulated and, u_l and $\dot{u_l}$ is orthogonal it would be stated as follow

$$\int_0^{R_{MT}}\vec{r}^2u_l\dot{u}d\vec{r}=0 \tag{61}$$

Coefficient A_L and B_L is decided satisfying spherical boundary condition of basis function ± and its differentiation $\frac{\partial\phi}{\partial\vec{r}}$. Similarly Z, dependency function $u_{k+G}(E_\nu,z)$ and differentiation of energy $\dot{u}_{k+G}(E_\nu,z)$ are derived by solution of one dimension Schrodinger equation like following equation.

$$[\frac{\partial^2}{\partial z^2}+2(E_v-V(z)-(\vec{K}+\overrightarrow{G^2})]u_{K+G}=0 \tag{62}$$

$$[\frac{\partial^2}{\partial z^2}+2(E_v-V(z)-(\vec{K}+\overrightarrow{G^2})]\dot{u}_{K+G}=0 \tag{63}$$

Continuous condition of ± and $\frac{\partial \phi}{\partial \vec{r}}$ on the boundary of vacuum will be used for deciding $A_v$and B_v.

In Method of FLAPW $n(r)$density of charge would be stated with 3 area as follow.

$$\begin{aligned} n(\vec{r}) &= \sum_G n_G\, e^{iG\cdot r} && r\in institial \\ n(\vec{r}) &= \sum_L n_L(\vec{r})\; Y_L(\hat{r}) && r\in MTsphere \\ n(\vec{r}) &= \sum_G n_G(z)\; e^{iG\cdot r} && r\in vacuum \end{aligned} \tag{64}$$

Coulomb potential could be derived with solution of Poisson equation and effective single particle potential which has been given in sum of Coulomb potential and correlation exchange potential would be represented with the form of density of charge given in (equation 64). Finally secular equation would be as follow.

$$\sum_{G'}[H_{G,G'} - \epsilon_i(\overrightarrow{k})O'_{G,G}]c_{i,k}(\overrightarrow{G'}) = 0 \qquad (65)$$

here, $H_{G,G'}$ is Hamiltonian matrix in K-S equation and $O_{G,G'}$ is overlap matrix.

As concept of linearization with Method of LAPW radial function could be developed from random E to term of $u_l(E_l)$ and $\dot{u}_l(E_l)$.

$$u_l(E) = u_l(E_l) + \delta\dot{u}(E_l) \qquad (66)$$

here, δ would be decided by coefficient of A_L and B_L in (equation 58) satisfying a boundary condition of Muffin-tin sphere.

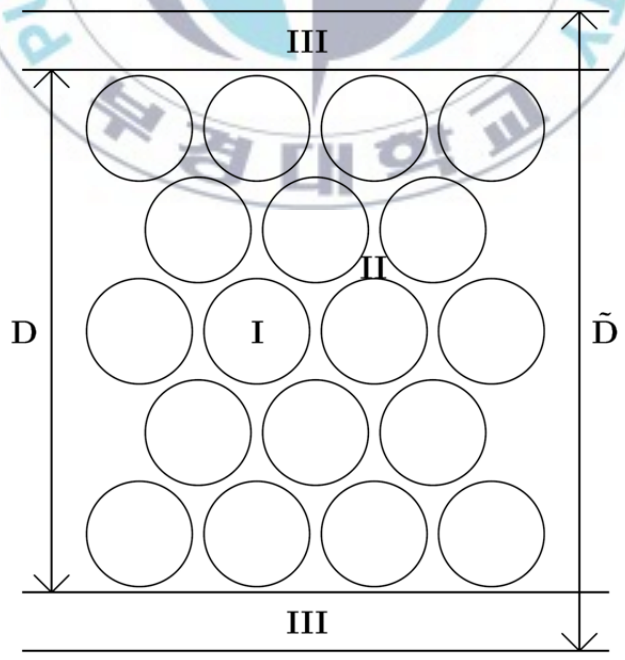

Figure 2. Schematic representation of the film geometry for film version FLAPW calculations. Region I, II, III denote the mun-tin(MT) sphere, interstitial, vacuum region, respectively.

4. Magnetic properties of low-dimensional structure

Low-dimensional magnetism of surfaces, interfaces and thin-films is currently an area of intense interest. Recently it has become possible to synthesize and study thin magnetic films with either stable or metastable phases. The FLAPW affords the calculation of surface magnetic properties such as magneto-crystalline anisotropy (MCA), magneto-optical Kerr effects (MOKE), as well as x-ray magnetic circular dichroism (XMCD) spectra. The spin-orbit coupling (SOC), which basically induces these phenomena, is treated in the second variational method [26] which is known to provide a precise as well as reliable result for the light transition metals and their compounds.

4.1 Spin-orbit coupling

Spin-orbit coupling leads to a number of important effects such as magnetic anisotropy and magneto-optical spectra. The SOC term given by

$$H_{SOC} = \frac{1}{4c^2}\sigma \cdot \nabla V \times p \tag{76}$$

couples spin-up and spin-down wave functions, which means $2N \times 2N$ secular equations if one begins (without SOC) with N basis functions and thus roughly eight times more computing time. Recognizing that

the SOC is generally a small effect for valence electrons, this difficulty can be avoided by using the so-called second variational method [30]. The second variational procedure is summarized as: (i) solve the scalar relativistic equation without the SOC term self-consistently for each spin; (ii) calculate the SOC Hamiltonian in the space of the low lying n scalar relativistic wave functions for each spin obtained in (i); (iii) solve the $2n \times 2n$ secular equation; and (iv) re-expand the new wave functions in terms of the initial $2N$ basis set.

Since, especially in the FLAPW method, the number of bands of interest, n, is always much smaller than the number of basis functions, N, used to solve it self-consistently, choosing the small n number of wave functions to describe the SOC Hamiltonian is very efficient even after the spin mixing doubles the matrix size. Further, in this second variational basis, the overlap matrix is diagonal and thus the total Hamiltonian matrix is given by the SOC matrix plus the scalar relativistic eigenvalues on the diagonal. Noting that the gradient of the potential yields its largest contributions inside the MT sphere where the potential is almost spherical, we can assume

$$\nabla V = \begin{cases} \dfrac{\vec{r}}{r}\dfrac{dV}{dr} & \text{for } |\vec{r}| < R_{MT} \\ 0 & \text{for } |\vec{r}| > R_{MT} \end{cases} \tag{77}$$

and therefore

$$H_{SOC} = \frac{1}{4c^2}\sigma \cdot (\vec{r} \times \vec{p})\frac{1}{r}\frac{dV}{dr} = \frac{1}{4c^2}\sigma \cdot L\frac{1}{r}\frac{dV}{dr} \qquad (78)$$

in the MT sphere. Then the SOC matrix elements are calculated by separating the angular and radial parts. Usually the SOC strength, ξ, is defined as the radial integral part of the SOC matrix element. This second variational approach is much more efficient compared to other approaches like the full relativistic scheme. But it''s deficiency is reported in Pb metal for the states with large $p_{1/2}$ components [30]. This is because the scalar relativistic FLAPW radial functions which vanish at r = 0 for l = 1 does not properly describe $p_{1/2}$ which, unlike $p_{3/2}$ or higher l orbitals, can have a finite amplitude at the nucleus and thus a possibly strong relativistic effect.

4.2 Magnetic anisotropy

The primary property of a ferromagnet such as Fe, Co, or Ni is the appearance of a spontaneous magnetization M below the Curie temperature Tc. Ferromagnetic materials exhibit intrinsic 'easy' and 'hard' directions of the magnetization. On this account, ferromagnetic material has the unique physical properties that is magnetic anisotropy. It is the directional dependence of a material's magnetic properties.

Like this, It can be described by two different interactions such as the magnetic dipolar interaction and the spin orbit interaction. It is important in various aspects of applications thermal stability, coercivity and perpendicular magnetic recording: and challenges for fundamental understanding.

Magnetocrystalline anisotropy (MCA)

The magnetocrystalline anisotropy (MCA) energy is defined as the difference of the total energy for two different magnetization orientations, for example, in-plane and perpendicular. To determine the magnetic anisotropy energy using first principle calculations, it requires great accuracy due to very small changes in total energies (e.g. of the order of a few tenths of meV/atom), and these differences arise mainly in regions of the band structure near band crossings and electron states near the Fermi level. For this reason huge number of k-points in the 2D Brillouin zone (BZ) may be required. The force theorem [27], state tracking [28] and torque methods [29] were proposed to solve these difficulties in MCA calculations and proved to provide reliable as well as precise results for many systems.

The force theorem, which starts from the variational expression for the total energy in density functional theory, shows that

【part 1】 Given an exact density, ρ_0, the total energy estimated from a trial density, ρ, is correct to the second order of the charge variation,

i.e.,

$$E[\rho] = E[\rho_0] + O[(\rho - \rho_0)^2] \tag{67}$$

【part 2】If there are two crystal structures, α and β, with charge densities, ρ_α and ρ_β, the difference in the total energy estimated from the respective charge densities, $E_\alpha[\rho_\alpha] - E_\beta[\rho_\beta]$, can be approximated as the difference in the sum of the single-particle eigenvalues due to systematic cancellation of other terms.

The force theorem can be applied to MCA calculations: In the second variational treatment of SOC, one starts with the scalar relativistic self-consistent charge/spin density, $\rho_0(r)$ and $m_0(r)$, and the corresponding scalar relativistic total energy, $E_0[\rho_0, m_0]$. If it is assumed that the scalar relativistic plus SOC calculations yield the charge/spin density ρ_r and $m(r)$ and the corresponding total energy $E[\rho, m]$, the SOC induced energy can be written as:

$$\begin{aligned} E_{sl} &= E[\rho, m] - E[\rho_0, m_0] \\ &= E[\rho, m] - E[\rho_0, m_0] + E[\rho_0, m_0] - E_0[\rho_0, m_0] \end{aligned} \tag{68}$$

According to 【part 1】, we see that the first bracketed term in (equation 68) is negligible to first order of the charge/spin density variations induced by SOC. On the other hand, the 【part 2】 ensures that the second bracketed term of (equation 68), which is the difference

in total energy with and without SOC estimated from the scalar relativistic charge/spin densities, can be approximated as the difference in two sums of single particle energies with and without SOC, as:

$$E[\rho_0, m_0] - E_0[\rho_0, m_0] \approx \sum_{ik}^{occ} \epsilon_i(\hat{m}, k) - \sum_{ik}^{occ} \epsilon_i^0(k) \tag{69}$$

From the force theorem, the MCA $\triangle E_{sl}$, defined as the difference of the total energy for in-plane $(\theta = 90^o)$ and perpendicular $(\theta = 0^o)$ magnetization orientations, can be written as:

$$\begin{aligned} \triangle E_{sl} &\equiv E(\hat{m}_{\theta=0}) - E(\hat{m}_{\theta=90}) \\ &= \sum_{ik}^{occ} \epsilon_i(m(\theta = 90^0), k) - \sum_{ik}^{occ} \epsilon_i(m(\theta = 0^0), k) \end{aligned} \tag{70}$$

The rotation of the magnetization from 0^o to 90^o leads to a redistribution of the occupied states and it has been noted that this may lead to a possible introduction of errors; a way to get around this was proposed which is called the state-tracking method [15]. In the state-tracking technique, $H^{sl}$is treated in a second variational way in the space expanded by Ψ_i, i.e.

$$< \Psi_i | H^0 + H^{sl} | \Psi_j > \; = \; \epsilon_i \delta_{ij} + < \Psi_i | H^{sl} | \Psi_j > \tag{71}$$

with the SOC perturbed state:

$$\Psi_i^{'} = \sum_j C_j^i \Psi_j \tag{72}$$

Here, ϵ_j and Ψ_j are eigenvalues and wave functions obtained for the unperturbed Hamiltonian, H^0, using the regular FLAPW method. The occupancy is determined by tracking its projection onto the occupied states by defining

$$P_i^{occ} = \sum_{j \in O} \left| C_j^i \right|^2 \tag{73}$$

Since H^{sl} is very weak, this definition does not introduce any ambiguity, i.e., the value of P_i^{occ} is either > 99% or <1%. In this sense, the newly occupied states give almost the same spatial distribution of the charge and spin densities which ensures the correct application of the force theorem. Furthermore, such a state-tracking procedure is done independently at each k point; hence, the randomness in the BZ can also be removed. More recently, the torque method [16] was proposed as another way to simplify MCA calculations by realizing that the definition of MCA is equivalent to the partial derivative of SOC energy with respect to θ calculated at $\theta = 45^o$. For example, for the surface with 4-fold rotational symmetry, where the ϕ dependence of the

MCA is negligible, and the SOC energy has the form $E_{sl}(\theta) = K^{(2)}\sin^2(\theta) + K^{(4)}\sin^4(\theta)$, then

$$T(\theta = 45^o) \equiv \left[\frac{dE_{sl}(\theta)}{d\theta}\right]_{\theta = 45^o}$$
$$= -K^{(2)} - K^{(4)}$$
$$= E_{sl}(\theta = 90^o) - E_{sl}(\theta = 0^o) \equiv \triangle E_{sl} \quad (74)$$

In practice, the torque is calculated by applying the Hellman-Feynman theorem as

$$T(\theta) \equiv \sum_{i,k}^{occ} < \psi_{ik} \left| \frac{\partial H_{sl}}{\partial \theta} \right| \psi_{ik} > \quad (75)$$

where ψ_{ik} is the wave function of the SOC Hamiltonian, H_{sl}. The advantage of the torque method is that there is only one Fermi energy to be estimated which suppresses the fluctuations due to the independently determined Fermi energies of the perturbed and the unperturbed states as mentioned above. The state tracking method still can be used to determine the new occupied states for the SOC Hamiltonian, an advantage that may not be critical. However, there is a trade-off in using the torque method; the magnetization oriented

along $\theta = 45^o$ reduces the symmetry for most systems, which results in a larger IBZ and thus an increased number of k-points.

4.3. X-ray Magnetic circular dichroism (XMCD)

X-ray Magnetic circular dichroism (XMCD) is useful for identifying the magnetism from different specific atoms, e.g., in alloys, impurities at surfaces or interfaces. Also for the potential application of element-specific magnetic microscopy. MCD measures the difference in absorption between right- and left-circularly polarized incident light during the process of electric transitions from core states to unoccupied valence states. Due to the spin-orbit coupling (SOC) between valence states, the MCD signals no longer cancel each other as they do in the absence of SOC where the signals are equal and opposite. The energy dependence of the cross sections, i.e., σ_+, σ_- and σ_z, (σ_+ and σ_- represent the absorption cross sections for left- and right-circularly polarized light, respectively) for electric dipole transitions from core to valence bands can be evaluated as

$$\sigma_n(E) = 8\pi^2/3 \int_k |< \psi_c | p_n | \psi_v^{'} >|^2 \delta(E_v - E_c - E) dk \quad n = \pm z \tag{79}$$

The angular and spin momentum parts of the p-matrices result in the well-known selection rules: $\triangle l = \pm 1$, $\triangle m = \pm 1, 0$ and $\triangle S = 0$.

5. Magnetism in boron nitride systems

5.1 Magnetism in boron nitride monolayer: adatom and vacancy defect

5.1.1. Introduction

Traditionally, it is believed that the 3d transition metal elements are essential for the realization of magnetism of material. However, recently the great research efforts has been focused on the possibility of magnetism from 2p electrons, so called d^0 magnetism, due to both device applications and fundamental interests. In particular, the magnetic property of carbon based hexagonal graphene system is of particular interest because the graphene system shows many extraordinary physical properties and the magnetic graphene may have many advantages for spintronic applications compared with other metallic materials or dilute magnetic semiconductors. Several studies have been performed to reveal the magnetic properties of graphene layer and in most of studies the influence of various types of defect has been considered, but the exact mechanism still remains an open question. Another interesting hexagonal system is a boron nitride film. As is well known, the hexagonal boron nitride and graphene systems are isoelectronic and the lattice constants are also very close to each other. For instance, the hexagonal graphite has a=b=2.46 Å, c=6.71 Å,

while the hexagonal boron nitride (h-BN) has a=b=2.50Å ,c=6.66 Å. Due to these similarities, the hexagonal boron nitride has also attracted extensive research interests for potential application purposes. One can find that many different types of nanostructured h-BN have been explored [31-34]. It is well known that the hexagonal carbon systems show different electronic structure according to the rolling type, for instance the carbon nanotube can display either metallic or semiconducting behavior. However, despite the isoelectronic with carbon based material, it is found that the h-BN systems show a wide band gap semiconducting feature [35]. On the other hand, like in the graphene system, it will be of interest to explore the magnetic property of the h-BN system for potential spintronic application as well. Indeed, the existence of magnetic state in the h-BN layer has been predicted by various theoretical studies. It is obvious that the pure h-BN has a finite band gap and it is non-magnetic. Thus, the issue has been focused on the defect induced potential magnetism in the h-BN layer. For instance, it has been shown that the B or N vacancy defect in the h-BN monolayer can bring a local magnetic moment [36]. As found in the carbon nanotube or nanoribbon systems, the possible magnetism due to the edge effect has also been suggested in one or two dimensional structure [37,38]. In addition, it is reported that the substitution or doping of light elements can induce a spin polarized state [39–42]. Along with the possibility of substitutional or vacancy

defect induced spin polarization, there may be another route to create magnetism in the h-BN due to adatom defect and no one has investigated the magnetic property arising from the adatom defect in the h-BN so far. Here, it should be remarked that we have studied the X-ray magnetic circular dichroism and found that the adatom defect may explain the possible magnetism in the pure graphene layer. As mentioned earlier, many previous theoretical studies indicate that the vacancy defect or substitutional defect may cause a spin polarized state, however the clear understanding for the magnetism in the h-BN has not yet been achieved. It should be noted that one cannot simply attribute the magnetism to the effect of vacancy defect or substitutional defect even if the theoretical calculations predict the existence of spin polarized state. To confirm the origin of magnetism in the h-BN layer, the mechanism predicted by first principles calculations should be verified via experimental measurements. Unfortunately, no one has ever reported the concrete experimental observation arising from the defect induced spin polarization in the h-BN layer. Thus the theoretical prediction does not necessarily imply that the origin of magnetism is understood although the potential spin polarization is suggested by theoretical studies. In this spirit, the two issues will be explored. First, we will calculate the influence of vacancy defect or adatom defect on the magnetic property of the h-BN monolayer. Second, we will find any indication whether the magnetic property of the h-BN monolayer

depends on the defect type. To this aim, the XMCD will be investigated along with the electronic structure study. We anticipate that these calculations will provide useful information to understand the origin of magnetism by comparison with future experimental observation. In particular, we believe that the calculated XMCD data will play an important role to extract the intrinsic source of spin polarization in the h-BN layer.

5.1.2. Numerical Method

The thin film version of full potential linearized augmented plane (FLAPW) method for magnetic properties is used. Therefore, no shape approximation is assumed in charge, potential, and wavefunction expansions [43-45]. We treat the core electrons fully relativistically, and the spin orbit interaction among valence electrons is dealt with second variationally [46]. The generalized gradient approximation is employed to describe exchange and correlation potentials [47]. Spherical harmonics with $l_{\max} = 8$ are used to expand the charge, potential, and wavefunctions in the muffin-tin region. Energy cut offs of 225 Ry and 13.7 Ry are implemented for the plane wave star function and basis expansions in the interstitial region. The supercell built by 4×4 cells is used. Thus, the lattice constant of 8.42 Å in lateral direction is employed and the calculated unit cell has 32 atoms in ideal structure. The muffin-tin radius of 1.2 atomic unit is used for both B and N

atoms. Since the central issue is to investigate the influence of defect due to adatom or vacancy on the magnetic property of h-BN monolayer, the vacancy defect system is simulated by removing a single B or N atom from its ideal site. On the other hand, the adatom defect configuration is prepared by introducing another B or N atom on top of BN sheet. In the case of adatom defect, there are several adsorption sites and we will calculate total energy at each possible adsorption point to find the most stable system. It is well known that the magnetic property may depend on subtle change in underlying electronic structure, therefore it is necessary to perform structure optimization. The optimized atomic structure is achieved through force and energy minimization procedure. The entire calculations have been performed with 38 k-points in irreducible Brillouin zone.

5.1.3 Result and discussion

We first explore the vacancy defect induced magnetic property of the h-BN monolayer. In Fig. 3, the schematic illustration of the h-BN sheet in the presence of B or N vacancy defect is displayed. The red ball stands for B(N) atom and the blue one is for N(B) atom, respectively. The vacancy site is denoted by a green ball. When the single N is removed, it is found that the B atom shows inward lattice distortion about 0.13 Å toward the N vacancy site (opposite direction to the arrow shown in Fig.3). In contrast, the B vacancy defect induces outward relaxation about 0.17 Å from its ideal position (along the

direction of arrow in Fig. 3).

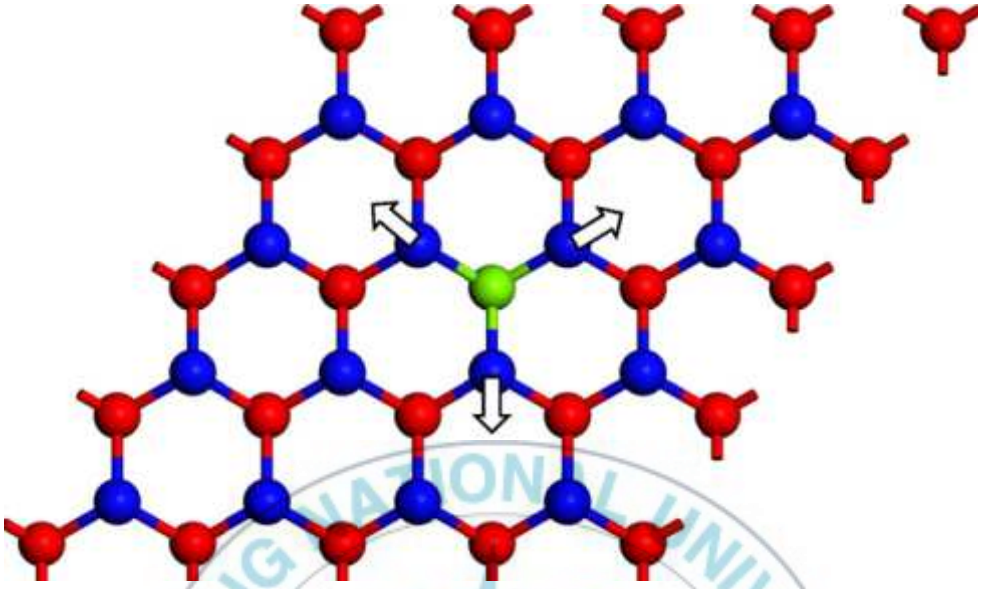

Figure 3. Schematic illustration of unit cell geometry of vacancy defect h-BN. The red ball stands for B atom and the blue one is for N atom. The vacancy defect is denoted by a green ball.

Through the vacancy defect formation energy calculations [35], we have found that the N vacancy defect formation is more favorable than the B vacancy formation by energy difference of 3.36 eV. This is similar to the previous theoretical calculation by Si et al. [36]. One may find that the B vacancy defect induces a magnetic moment which is much larger than $1\mu_B$ [36,41], meanwhile the N vacancy defect brings a magnetic moment of $1\mu_B$ [36,37]. In addition, it has been shown that both B and N vacancy defect systems manifest very close to half metallic feature. However, for the magnetic property of two dimensional h-BN monolayer, our results are fundamentally different from those found in the previous pseudo potential calculations. In our full potential

calculations, it is found that the N vacancy defect system shows no indication of meaningful spin polarization in B or N atoms at all. On the other hand, in the resence of B vacancy defect we have obtained that the three nearest neighbor N atoms around the B vacancy site have a magnetic moment about $0.29\mu_B$ per N atom, thus the total magnetic moment is about $0.78\mu_B$. It is claimed that the unit cell size does not affect the magnitude of spin magnetic moment [23], thus we believe that this fundamental disparity stems from the different treatment in the interaction among electrons, not due to the different size of unit cell. Note that the lattice distorted structure due to the vacancy defect is clearly more stable than the non-distorted case. For example, the energy difference in B vacancy defect is about $298meV$ and it is about $166meV$ in N vacancy defect configuration. In B vacancy defect without lattice distortion, the induced magnetic moment is $0.36\mu_B$, while there is no induced spin polarization in ideal N vacancy defect structure. As a result, we conclude that the existence of magnetic state is not essentially affected by the lattice distortion although the magnitude of magnetic moment is rather affected. We now present the results of adatom defect systems. In Fig. 4, the structure considered in our calculations is shown. The adatom is described by a yellow ball and the rest of them are similar as shown in Fig. 3. Since there are several possible adsorption positions, we have considered different configurations and they are labeled by numbers in

Fig. 4.

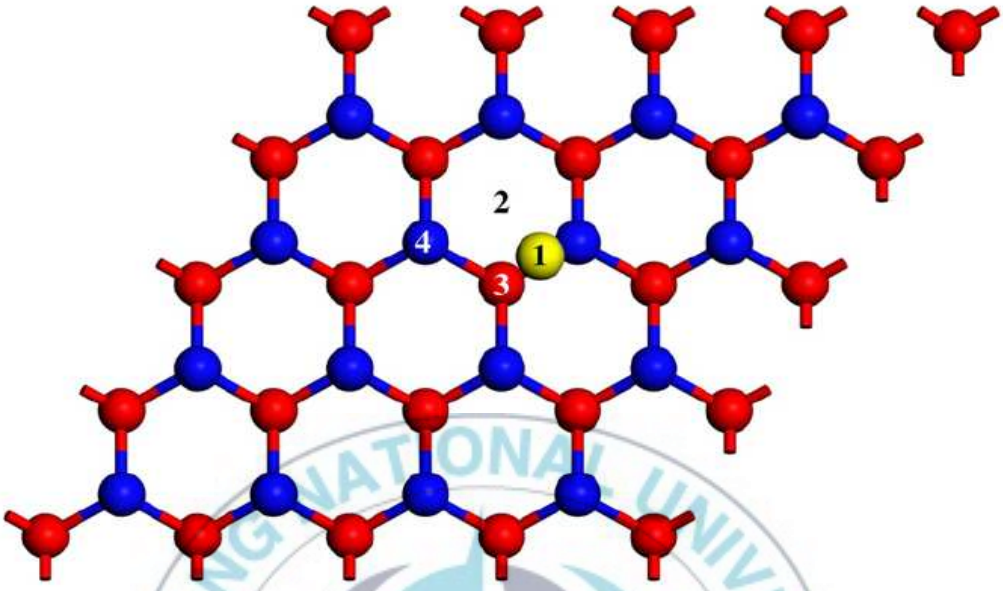

Figure 4 Schematic illustration of unit cell geometry of adatom defect h-BN. The red ball stands for B atom and the blue one is for N atom. The adatom defect is denoted by a green ball. The possible adsorption site is represented by a number.

In Table 1, we show the calculated total energy, magnetic moment, and vertical distance from the BN sheet according to the adsorption position and defect type. The total energy of bridge site, denoted by 1 in Fig. 4 is set to zero for reference. It is clearly obtained that the bridge site is the most stable adsorption position for both B and N adatom defects. This feature is the same as that found in the pure graphene system. It appears that the B adatom is spin polarized, but the magnitude of moment is rather weak and there is no induced spin polarization found in substrate atoms. Also, the magnetic moment is insensitive to the

adatom site although the total energy is quite different. In N adatom configuration, however, the magnetic moment is strongly sensitive to the adsorption site. In the most stable position, we still observe a sizable magnetic moment about $0.38\mu_B$. Nonetheless, there is no induced magnetic moment in the h-BN substrate layer.

	Bridge (1)	Hollow (2)	B top (3)	N top (4)
B adatom				
Energy	0	417	299	303
Moment	0.12	0.17	0.13	0.14
Distance	1.79	2.50	1.94	2.19
N adatom				
Energy	0	240	197	195
Moment	0.38	1.22	1.23	1.23
Distance	1.49	2.83	3.34	3.36

Table 1. Calculated total energy (in meV), spin magnetic moment (inμ_B), and vertical distance (in Å).

To check the stabilization of adatom system, the adsorption energy in each configuration is calculated. The adsorption energies of B and N adatom defect systems are $223meV$ and $731meV$, respectively and this indicates that one may be able to materialize the B or N adatom adsorbed system. In addition, the FM state of B atom system is more stable than paramagnetic phase and the energy difference is about 253 meV. In N adatom case, we have found similar result and the energy gain by FM spin polarization is $528meV$. The energy difference is very large, thus the spin polarized state may survive even in the presence

of small thermal fluctuation. Nonetheless, the quantitative critical temperature should be estimated by considering the property of exchange interaction when the two adatom defects are on the h-BN layer. In order to do that, it is necessary to increase the cell size to avoid artificial interaction with another defect in adjacent unit cell. We will explore this issue elsewhere although it is computationally very challenging task because of large unit cell size. Since the N vacancy defect has no influence on the magnetic property of h-BN, we first show the density of states (DOS) features of B vacancy defect system.

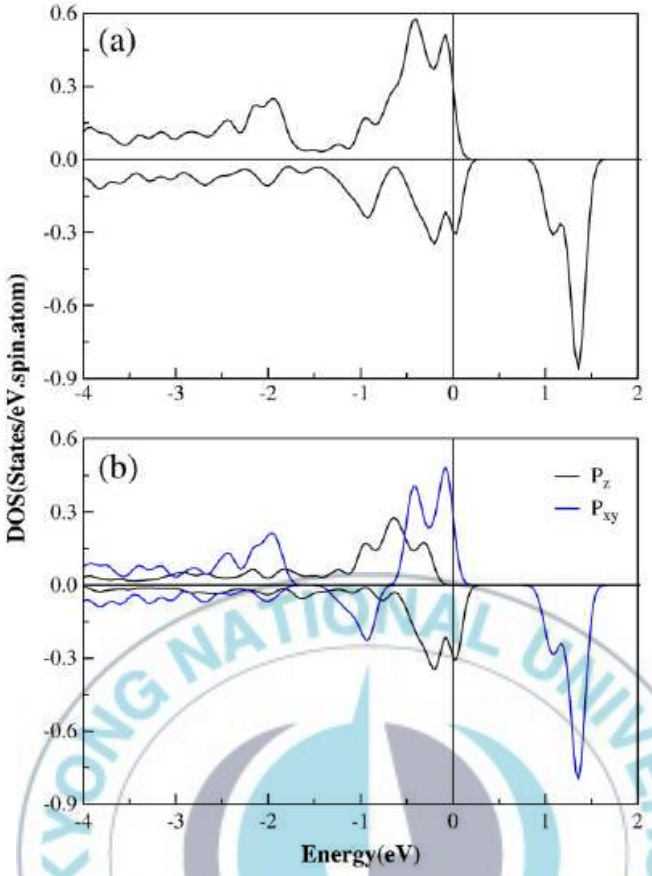

Figure 5. DOS of spin polarized N atom in the presence of B vacancy defect system ; (a) to 2s and 2p electrons and (b) m-resolved DOS of 2p electron.

In Fig. 5(a) and (b), the total DOS from $2s$ and $2p$ electrons and m-resolved DOS of $2p$ electrons are presented. First of all, the metallic DOS feature is found because one can see finite number of available states in both spin states at the Fermi level. We have further analyzed and realized that the essential spin polarization is definitely originated from the $2p$ electron. Moreover, it is observed that the major spin polarization stems from the $p_{x,y}$ as shown in Fig. 5(b), although one can still see weak spin polarization in the p_z state. This is quite different character from that found in pseudo potential calculations

because the half metallic state is observed [36,41].

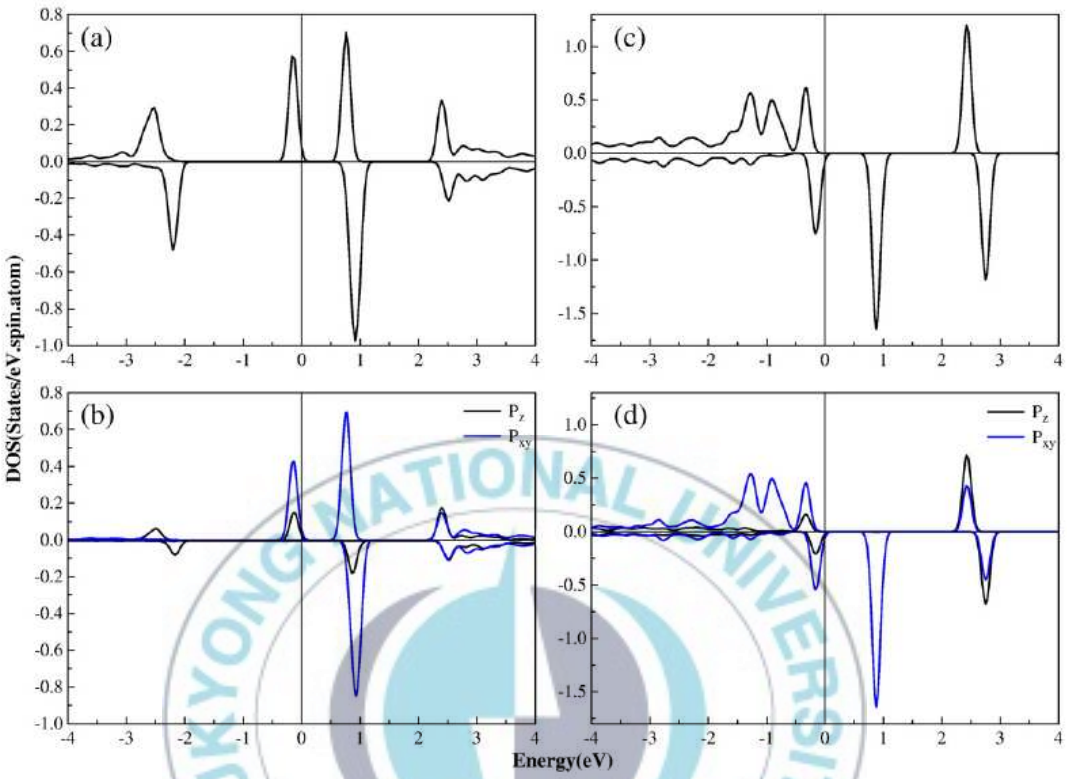

Figure 6. Calculated (a) total DOS from $2s$ and $2p$ electrons in B adatom, (b) m-resolved DOS in B adatom, (c) total DOS from $2s$ and $2p$ electrons in N adatom and (d) m-resolved DOS in B adatom.

In Fig. 6(a) and (b), the total DOS due to the $2s$ and $2p$ electrons and m-resolved DOS of $2p$ electrons in the presence of B adatom are shown, respectively. For the N adatom case, the similar results are shown in Fig. 6(c) and (d), respectively. In B adatom structure, strictly speaking, it shows a half metallic feature since the Fermi level resides in the majority spin state, while the minority spin state is empty at the Fermi level. However, there are only very few available majority

spin states at the Fermi level, thus it almost behaves like a pseudo semiconductor with a majority spin band gap about 1eV, while the minority spin band gap is about 3eV. We also find relatively large spin polarization in the $p_{x,y}$ state. In N adatom, the opposite DOS is observed at the Fermi level as shown in Fig. 6(c) and (d). The majority spin state at the Fermi level is empty, whereas one can see the tail of minority spin states. Besides, the band gap in each spin state is reversed as well. Like in the previous two cases, the major spin polarization occurs in the $p_{x,y}$. Overall, we have found that the three different systems display very different trends in their DOS features, in particular near the Fermi level. This finding may provide useful information to understand the origin of magnetism in h-BN in the near future. For instance, if one measures the defect induced spin polarized state using the surface sensitive experimental tool such as spin dependent scanning tunneling microscopy, the origin of magnetism will be understood by comparison with our theoretical results. In the study of magnetic materials, the XMCD can provide element specified magnetic information of materials. Therefore, it has been considered as an important tool in the study of magnetic materials. As shown earlier, we have found that the m-resolved DOS feature depends on the defect type. Thus, one may anticipate that the XMCD spectral shape will show different behavior and this XMCD data will be more informative rather than DOS for the origin of spin polarization. We thus present

the theoretically calculated XAS and XMCD in each system. Since the magnetic state is obviously originated from the $2p$ electrons, the K edge spectrum should be considered. Weonly take into account dipole transitions and the Doniach–Sunjic shape with 0.45eV for life time broadening has been employed [49]. The normal incidence to the film surface with circular polarization is assumed. In consequence, the XMCD spectrum is observable only in $\Delta m=\pm 1$ selection. In other words, the pz state does not contribute to the XMCD spectrum. In addition, it is assumed that the core-hole relaxation is rigid, therefore the exact peak position may be shifted if one wants to compare the energy level with experimental data.

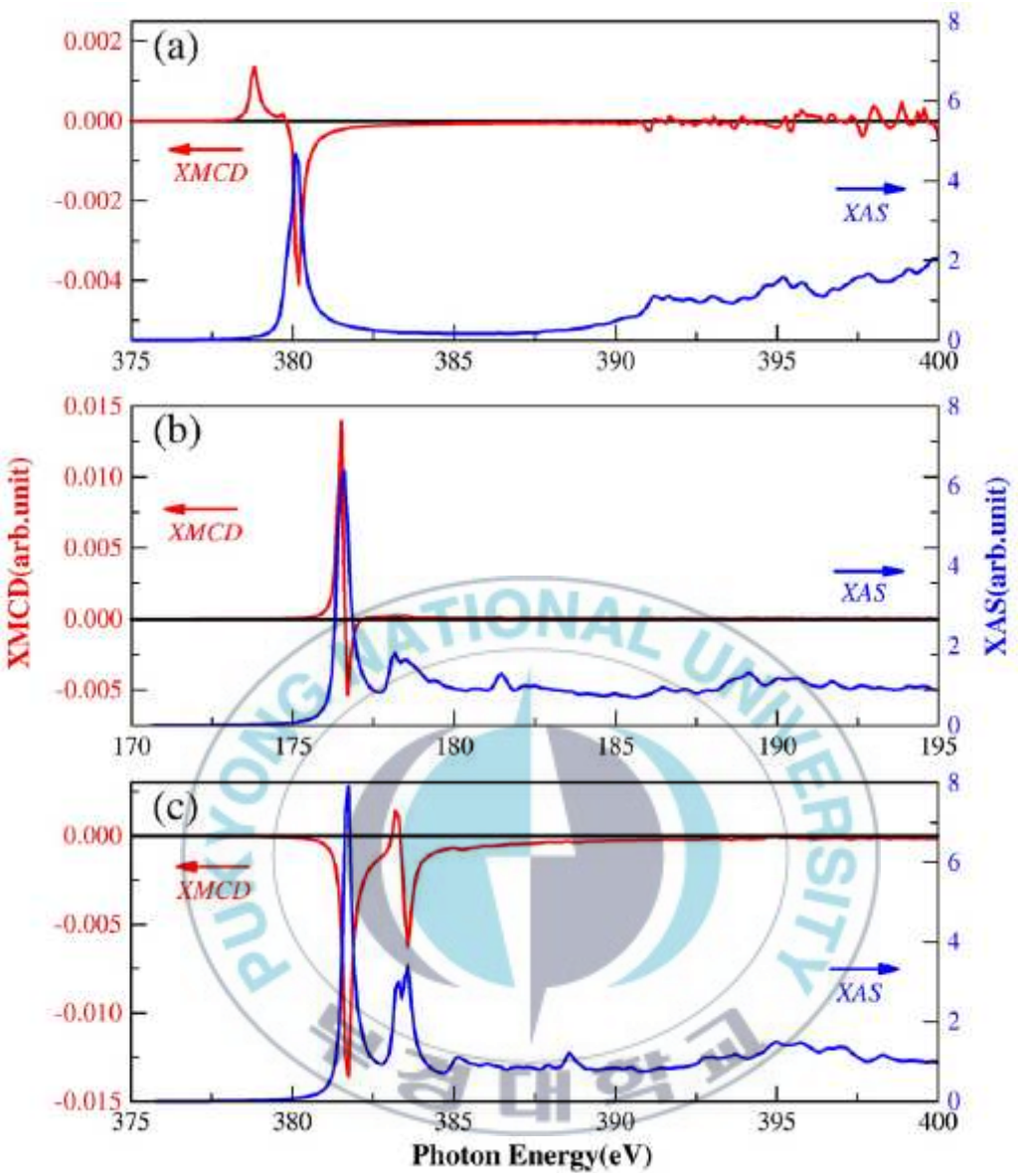

Figure 7. Calculated XAS and XMCD spectral shapes of (a) B vacancy defect, (b) B adatom defect and (c) N adatom defect. The blue line displays calculated XAS and the red one is for XMCD.

In Fig. 7(a), (b), and (c), we show the calculated results for the B vacancy defect, B adatom defect, and N adatom defect, respectively. The blue line stands for the XAS spectrum with right scale and the red one is for XMCD spectrum with left scale. One may see rather simple XMCD spectrum and this can be easily understood from the

calculated m-resolved DOS in Fig. 6(b). First of all, unfortunately it appears that the magnitude of XMCD is quite small compared with that of XAS. This implies that it is necessary to have high resolution XMCD tool to observe the signal. It is found that the onset energy of B adatom system in Fig. 7(b) is very different from that of N adatom or B vacancy defect. This fact is rather straight forward to understand because the atomic energy levels of B and N atoms are quite different. Therefore, it will be relatively easy to identify the source of spin polarization if the magnetic state occurs in B atom. However, if the spin polarization comes from the N atom, it is hard to tell whether the spin polarization is due to the N adatom or B vacancy defect with the electronic structure study only because both defects result in spin polarization in N atom. In this case, the XMCD spectral shape will help distinguish the origin of magnetic state in the h-BN monolayer. As presented in Fig. 7(a) and (c), the XMCD spectral shapes show different behaviors. For instance, the positive onset occurs followed by another single negative signal in B vacancy defect. In N adatom, we have two negative XMCD spectra with negative onset. Interestingly, there is a positive peak in between two negative signals. From Fig. 7(b), one can see the majority px,y above the Fermi level and the onset of minority spin states is found in 1 eV above Fermi level. This can explain the well separated two peaks in Fig. 7(a). In the presence of N adatom as shown in Fig. 6(d) for the N adatom case, two separate

minority spin states are observed at 0.8eV and 2.8eV in empty states. Moreover, we find the majority states at 2.5eV above the Fermi level. The positive XMCD peak in N adatom configuration results from this m-resolved behavior. Overall, these m-resolved DOS characters can nicely account for the disparity in XMCD spectral shapes according to the defect type.

5.1.4. Summary

In conclusion, we have explored the possibility of defect induced magnetism in the h-BN monolayer. It has been observed that the B vacancy defect can induce a spin polarization of $0.29\mu_B$ in N atom, while the N vacancy defect has no influence on the magnetic property. In the presence of adatom defect, the N adatom is spin polarized with a magnetic moment of $0.38\mu_B$, but the B adatom is weakly spin polarized with a magnetic moment of $0.12\mu_B$. It is found that the DOS in vacancy defect configuration shows metallic state and this is a quite different result compared with the results with pseudo potential calculation. In adatom defect, the spin polarized atoms preserve very similar to the semiconducting feature since the finite energy gap is observed. Through the XMCD calculations, we also obtain that the spectral shape of spin polarized B or N atoms displays different behaviors. Overall, it is realized that the theoretically calculated DOS and XMCD results are strongly sensitive to the defect type. If one

finds any indication of spin polarized state through clear experimental observation in the near future, the experimental data can be compared with our theoretical predictions. Thus, we believe that our results may provide the useful information regarding the intrinsic property of magnetism in the h-BN monolayer.

5.2 Potential room temperature ferromagnetic O/BN and F/BN bilayers

5.2.1 Introduction

There is much research interest in observations of magnetic moments in materials without any $3d$ transition metal elements, so-called d^0 magnetism, due to both fundamental properties and potential device applications. To date, many different types of materials have been investigated [50-53]. In this d^0 magnetism it is believed that the $2p$ electrons play a major role. Regarding d^0 magnetism, the most attractive material is a carbon-based hexagonal graphene system because graphene shows many extraordinary physical properties and magnetic graphene may have many advantages for spintronics applications compared with other metallic materials or dilute magnetic semiconductors. One may find studies of the magnetic properties of graphene or carbon-based materials in [54-56]. Along with the graphene layer, the boron nitride (BN) system is an intriguing structure as well. Three different types of structures such as hexagonal BN (h-BN), cubic BN, and wurtzite BN can be found. Among them, the one monolayer of h-BN is of particular interest since both graphene and h- BN are isoelectronic and the lattice constants are very close to each other. Therefore, various types of nanostructured h-BN have been explored [33,34,58]. Despite the structural and isoelectronic similarity, the h-BN

is a wide band gap material [35], whereas the carbon-based nanotube displays metallic or semiconducting behavior according to the rolling type. Besides the electric properties, many studies have been performed to find potential magnetism in an h-BN layer. It is obvious that the ideal BN layer shows a non-magnetic feature and has a finite size band gap, but it has been proposed that the h-BN may have a spin polarized state owing to vacancy defects, the edge effect, or the doping effect [59-62,39-41]. Nevertheless, no one has ever reported clear experimental observations arising from the defect-induced magnetism. From a practical point of view, the defect-induced magnetism may have some obstacles for spintronics application purposes since the defect induced magnetic properties may substantially depend on the defect type, relative distance between defects, and defect concentration and it is unlikely to control such issues to obtain desirable physical properties. In contrast, one can quite easily grow two-dimensional multilayer systems. In this spirit, we will explore the potential magnetism of an h-BN layer in the presence of 0.5 monolayer fluorine (F) and oxygen (O) adlayer. We will also study whether the room temperature ferromagnetic h-BN bilayer system is achievable.

5.2.2. Numerical method

The thin film version of the full potential linearized augmented plane (FLAPW) method for magnetic properties is used. Therefore, no shape

approximation is assumed in charge, potential, or wavefunction expansions [43–45].We treat the core electrons fully relativistically, and the spin–rbit interaction among valence electrons is dealt with variationally [46]. The generalized gradient approximation is employed to describe exchange and correlation potentials [47]. Spherical harmonics with $l_{\max} = 8$ are used to expand the charge, potential, and wavefunctions in the muffin-tin region. Energy cut offs of 324 Ryd and 16 Ryd are implemented for the plane wave star function and basis expansions in the interstitial region. The supercell built by 2 × 2 cells is used to simulate 0.5 monolayer O and F adsorption on the BN layer. Thus, a lattice constant of 5.04Å in the lateral direction is employed. The muffin-tin radius of 0.69Å is used for all atoms. The optimized atomic structure is achieved through a force and energy minimization procedure. All the calculations have been performed with 406 k-points in the irreducible Brillouin zone.

5.2.3. Result and discussion

In figure 8(a), we present the schematic illustration of an h-BN sheet with a 0.5 monolayer of F or O adlayer. Here, the 2 × 2 cell is drawn to take into account the antiferromagnetic configuration. The 1×1 unit cell is represented by a solid line. A red (gray) ball stands for an N atom and a yellow (white) one is for a B atom, respectively. The adlayer is represented by a blue (black) ball. There are four possible

adsorption sites: B-top, N-top, hollow, and bridge sites, although only the B-top site is illustrated in this figure. We first calculate the most stable configuration through the total energy method. Of course, it is required to check whether the bilayer structure can be made by calculating the adsorption energy.

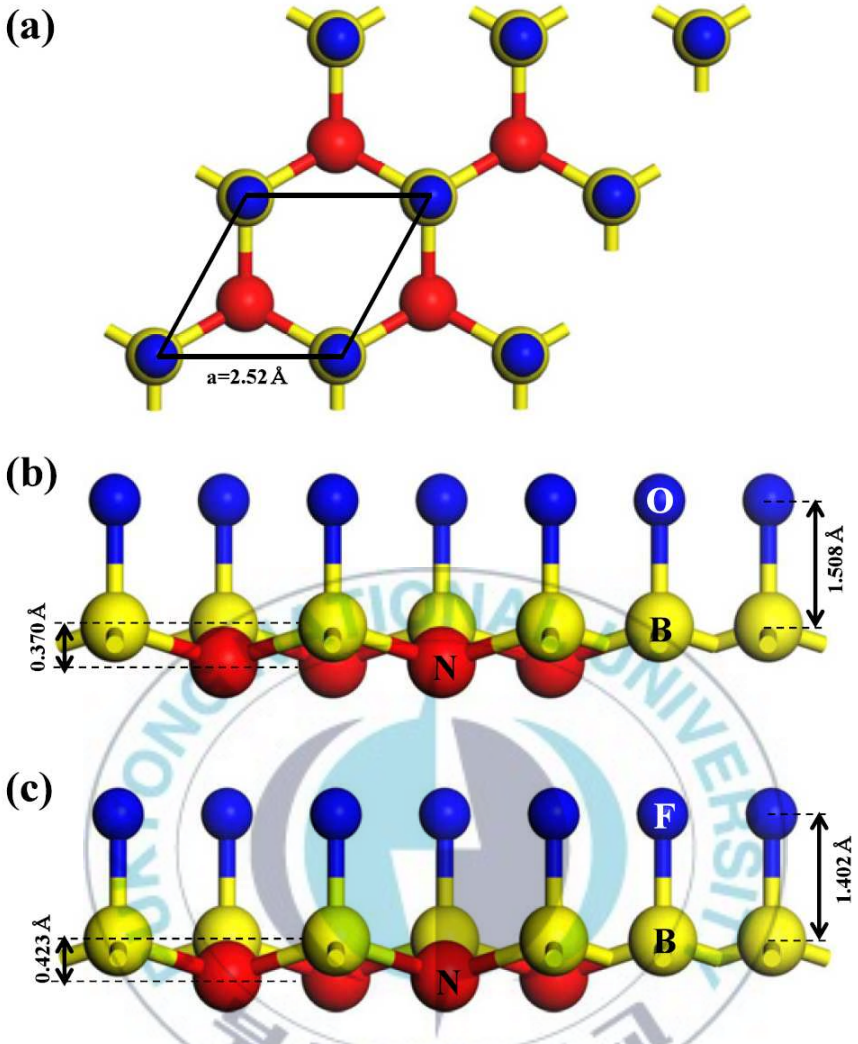

Figure 8. Schematic illustrations of (a) the unit cell, (b) the side view and optimized structure of O/BN, (c) the side view and optimized structure of F/BN.

In table 2, we present the total energy according to the adsorption site. Note that the calculations are performed with a 2 × 2 supercell, but the energy difference is expressed with a 1 × 1 unit cell. In the F/BN system, we have found that the F adlayer can only be adsorbed on N-top or B-top sites. For instance, if the F adatom is placed on a bridge site, it moves to the B-top position. Through adsorption energy

calculations, we find that adsorption on a hollow site cannot be realized. The most stable structure is achieved on a B-top site and the ferromagnetic (FM) ground state is observed. One can see quite different behavior in the O/BN structure than in the F/BN system. Nonetheless, we find that the O/BN also has a FM ground state. Note that the calculated adsorption energies in the ground state are $601meV$ and $1116meV$ for O/BN and F/BN, respectively. Overall, both F/BN and O/BN display the FM ground state on the B-top site. In figures 8(b) and (c), we show the optimized structure of O/BN and F/BN in the ground site, i.e. the B-top configuration. One can see that the BN monolayer manifests rippling surface geometry. In both cases, downward relaxation in the N atom (red/gray) is seen. The distance between F–B is about 1.402Å
and the distance between O–B is 1.508Å . One can know that the bonding strength of F–B is stronger than that of O–B and this agrees with the calculated adsorption energy. Besides the FM ground state, it has been found that both O/BN and F/BN systems maintain a very close to half-metallic band structure and this will be presented later.
One may find that the pseudo-potential calculation suggests that the F/BN system has an antiferromagnetic ground state with a finite band gap [25]. This is a fundamentally different result from that found via the full potential method. We believe that this feature stems from the different approach for treating interaction among electrons. In O/BN,

the calculated spin magnetic moments of O and N atoms in the muffin-tin area are 0.91 and $0.40\mu_B$, respectively. In F/BN, the N and F atoms have magnetic moments of 0.44 and $0.18\mu_B$, respectively.

	FM	AFM	PM
O/BN			
B-top	0	184	425
N-top	492	Not adsorbed	Not adsorbed
Hollow	506	Not adsorbed	505
Bridge	477	Not adsorbed	Not adsorbed
F/BN			
B-top	0	24	254
N-top	850	969	1101
Hollow	Not adsorbed	Not adsorbed	Not adsorbed
Bridge	Move to B-top	Move to B-top	Move to B-top

Table 2. Total energy according to adsorption site and magnetic state (in meV).

There is no induced magnetic moment in any B atom. For potential spintronics device application purposes, it will be of particular interest if the room temperature ferromagnetic system is found. The exact quantitative calculation of the Curie temperature may require more extensive study, but we can roughly estimate the possible range of Curie temperature based on a rather simple meanfield model. It is given by $T_c = 2 \times \frac{E_{AFM} - E_{FM}}{k_B \zeta}$, where k_B is a Boltzmann constant and ζ is a constant representing the dimensionality of the system. If we

assume that the bilayer systems have three-dimensional interaction, the Curie temperature of F/BN is about 185 K. Very interestingly, one can see that the Curie temperature is about 1423 K in the O/BN structure. Indeed, it is well known that the experimentally observed critical temperature is lower than the mean-field prediction by roughly a factor of two in many systems. Nonetheless, our calculated result implies that the O/BN system is very promising as a potential candidate for room temperature FM bilayer systems even if the critical temperature deviates from the mean-field prediction.

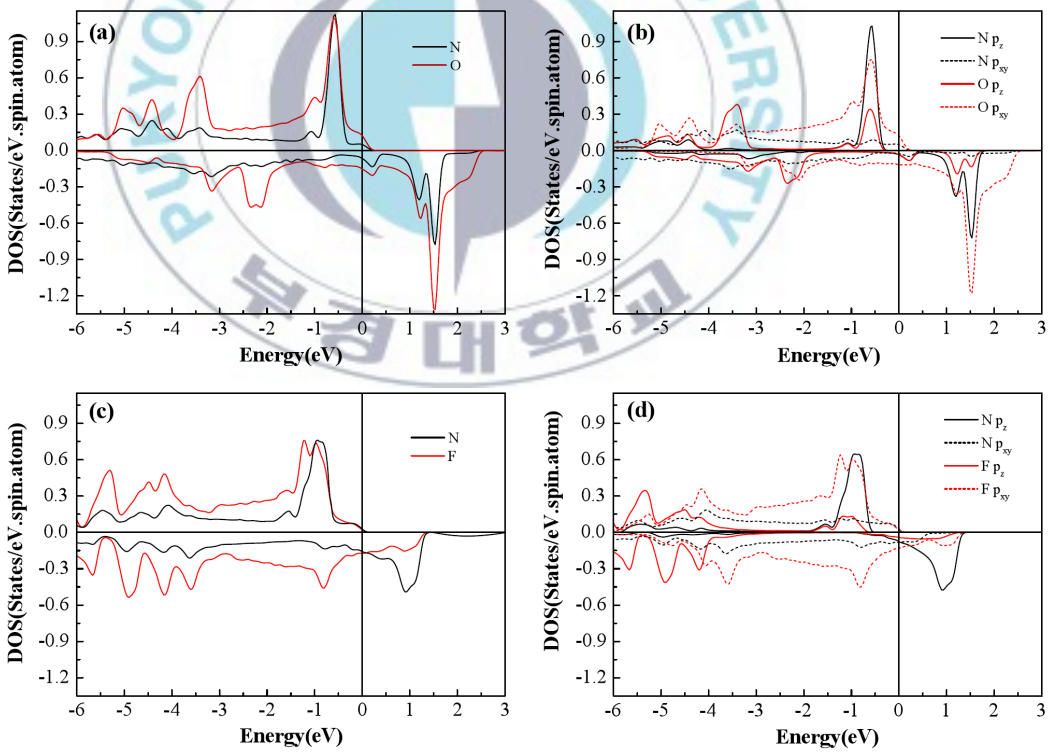

Figure 9. (a) DOS of O and N in O/BN, (b) m-dos of O and N in O/BN, (c) DOS of F and N in F/BN, (d) m-dos of F and N in F/BN.

In figures 9(a) and (b), we show the total density of states (DOS) and m-resolved DOS of the $2p$ state of the O/BN system. The DOS features of F/BN are shown in figures 9(c) and (d). In figure 9(a), one can see that both O and N atoms show metallic behavior with noticeable spin asymmetry. This results in large spin magnetic moments in O and N atoms. In figure 9(c), the DOS of F/BN is very close to the halfmetallic state. In addition, the spin asymmetry in the F adlayer is greatly suppressed compared with that of the O adlayer in O/BN, while one can still see the spin magnetic moment in the N atom. We have further analyzed the DOS to understand the major contribution to the spin polarization. In figure 9(b), the m-resolved DOS of O and N atoms is presented. For oxygen, the essential spin magnetic moment stems from the $p_{x,y}$ state, while the p_z state is weakly spin polarized. However, we have found the opposite behavior in the N atom. The spin asymmetry of $p_{x,y}$ is almost negligible. In contrast, one can see large spin asymmetry in the p_z state. In F/BN, the magnitude of the spin magnetic moment is rather small, but in general a similar trend has been found. For instance, the magnetic moment of the F adlayer is mainly due to the $p_{x,y}$ state, whereas the p_z state mostly contributes to the magnetic moment of the N atom. Overall, we have found that the spin polarization vanishes along the bonding direction, whereas the unpaired state in the non-bonding direction and the spin magnetic

moment is observed due to this feature.

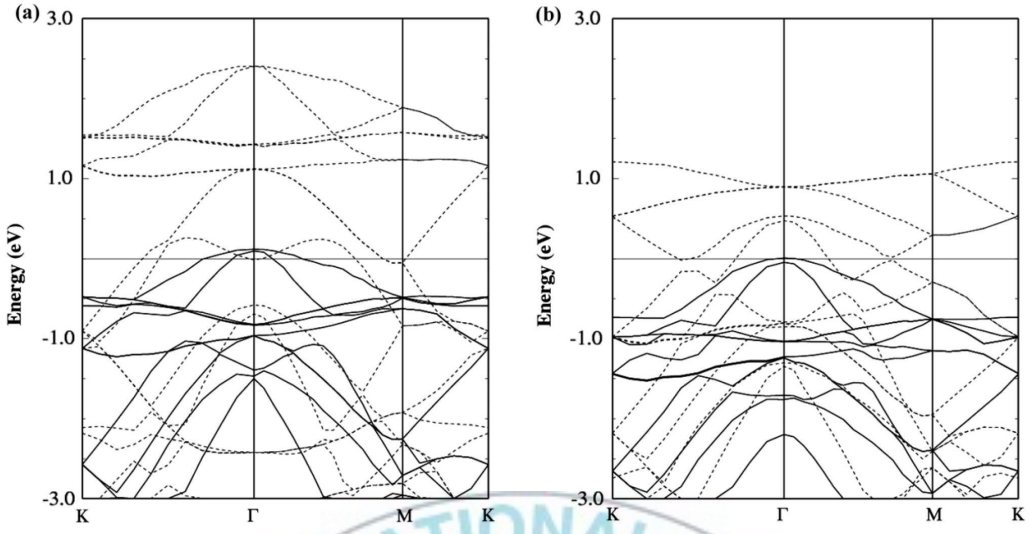

Figure 10. Calculated band structures of (a) O/BN, (b) F/BN. The solid lines are for majority spin bands and the dotted lines are for minority spin bands. The horizontal line represents the Fermi level.

In figures 10(a) and (b), we present the calculated band structures of O/BN and F/BN, respectively. Solid lines are majority spin bands and dotted lines are minority spin bands. As mentioned earlier, the one ML of pure h-BN is a wide band gap material, but both bilayer systems display metallic features. In particular, the F/BN is very close to the half-metallic state since the majority spin band slightly touches the Fermi level at the point. As remarked earlier, the pseudo-potential calculations have suggested that the F/BN has a direct band gap at the point [50], but here we have a fundamentally different result.

Since there is no clear experimental verification regarding the magnetism of the F/BN or O/BN bilayer systems, this disparity

should be verified via clear measurements in the near future. The XMCD technique provides very useful magnetic information about materials. Thus, we have investigated the XAS and XMCD spectral shapes. Since the magnetic state obviously originates from 2p electrons, the K edge spectrum should be considered. We only take into account dipole transitions and the Doniach–unjic [51] shape with 0.3 eV for lifetime broadening. Since normal incidence to the film surface is assumed, the XMCD spectrum is observable only due to the $m = \pm 1$ transition. In other words, the p_z state does not contribute to the XMCD spectrum. In addition, it is assumed that the core–hole relaxation is rigid, therefore the exact peak position may be shifted if one wants to compare the energy level with experimental data. As shown in the m-resolved DOS, the unoccupied $p_{x,y}$ states of the N atom in N/BN and F/BN are quite small and indeed the ratio of the XMCD peak to the XAS intensity was about 10^{-3}. Thus, we only present the XAS and XMCD of O in O/BN and F in F/BN structures. In figure 11, the blue dashed line is XAS and the red continuous line is XMCD. One can see that the XMCD of F in F/BN has a simple single peak feature with a single negative, whereas the O in O/BN is positive with double peaks followed by a negative peak. In figure 10(b), we have found that the magnitude of the majority spin $p_{x,y}$ DOS of the O atom at the Fermi level is larger than that of the minority spin state, while the opposite behavior is found in the F atom. Thus, the opposite of the

XMCD spectra can be understood. In addition, the double peaks in XMCD can be explained by the double-peak feature of $p_{x,y}$ of the O atom.

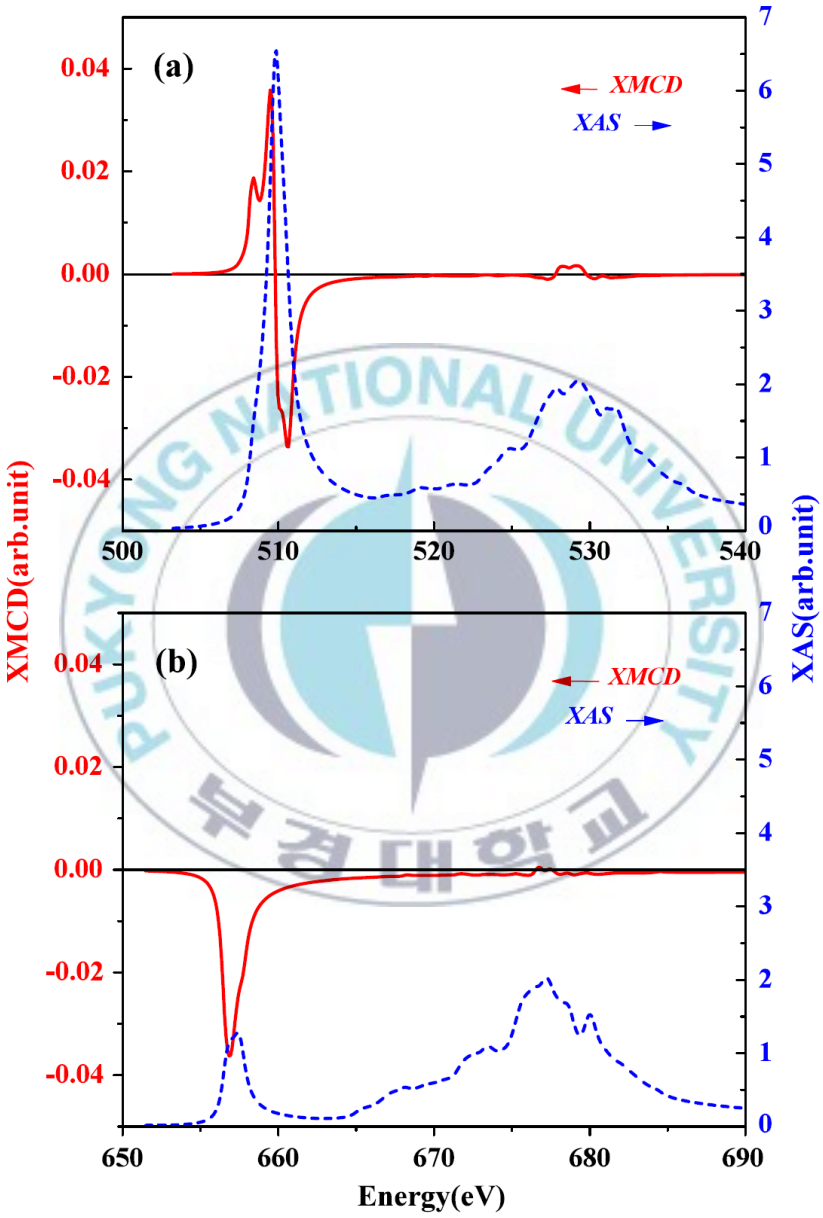

Figure 11. Calculated XAS and XMCD spectra (a) O in O/BN, (b) F in F/BN. The blue lines are for XAS and the XMCD is represented by red lines.

5.2.4. Summary

In conclusion, we have explored the potential magnetism of O/BN and F/BN systems. It is found that the O and F adlayers are adsorbed on the B-top site in both systems and an FM ground state with metallic behavior is predicted. In O/BN, the calculated spin magnetic moments are 0.91 and $0.4\ \mu_B$ for O and N atoms, respectively. In F/BN, it is found that the spin magnetic moment of the F adlayer is greatly reduced, while the N atom still maintains $0.44\ \mu_B$. It appears that the unpaired state exists in the non-bonding direction and this results in a spin magnetic moment. Through band structure studies, we find a clear metallic state in O/BN, while the F/BN shows nearly half-metallic features. Very interestingly, we propose that the O/BN is likely to display a potential room temperature FM state although the Curie temperature is estimated by a simple mean-field prediction. We have also presented the calculated XAS and XMCD spectra.

6. Magnetism based on graphene system

6.1. Carrier-induced spin switching in Co/Graphene/Ni: a first principles study

6.1.1. Introduction

The discovery of graphene [69] has led to extensive research efforts for both fundamental interests and innovative device application purposes. The graphene layer is well known to display extraordinary physical properties such as high mobility, a massless property at the K point, quantum hall effect [70,71] and can most likely to be used for novel device applications. Thus, study of the physical properties of the graphene system has become one of the most essential issues in condensed matter physics. So far, many studies have focused on the electric properties of graphene systems since the ideal graphene is non-magnetic. It will be of particular interest if the physical property of graphene layer can be utilized for spintronics purposes. However, the carbon based pure hexagonal graphene layer is non-magnetic since there is no unpaired electron in carbon atom. Regarding the magnetism in graphene, boron nitride layer, or some other materials, the role of vacancy or adatom defect has been discussed, but the origin of magnetism due to defects is still debating issue [72–75]. Further more,

it is rather difficult to control the magnetism arising from the defects since the magnetic state will be affected by various factors such as relative distance between defects, defects concentration, or adsorption sites. These obstacles should be avoided for spintronics applications. The multilayer system combined with magnetic layer will be an alternative way for spintronics purposes. In this respect, the graphene/Ni or graphene/Co system receives great research effort because the lattice mismatch between Ni(111) and graphene layer (Ni/Gr) or face centered cubic (fcc) Co layer and graphene (Co/Gr) is quite small. In this structure, various issues have been studied such as the Rashba effect, the adsorption structure, the electronic, or the magnetic properties [76–80] and mostly the ground state properties of Ni/Gr or Co/Gr have been investigated; for instance the magnetic moments, the band structures, or the structural information. One may note that the magnetic state can be tuned by using a field-effect-transistor geometry or by external doping in dilute magnetic semiconductors and both effects are achieved primarily via changes in the carrier density in semiconductor host. Here, it is presented that the carrier types can be controlled by external field [81–83]. Electric control of a magnetic state may open new opportunities for novel device applications. On the theoretical side, it has been demonstrated that the magnetic ordering in the delta doped (Ga,Mn)As system can be manipulated by external carrier [84]. Despite the large volume of

studies on the magnetic properties in graphene involved systems, it is rare to find the calculations for potential switching of magnetic interaction in trilayer system including graphene material [85]. Therefore, we will first explore the fundamental magnetic property of trilayer system. Based on this result, we will investigate the influence of external carrier type and concentration on the magnetic exchange coupling between two magnetic layers. We expect that we will be able to control the external carrier manipulation by applying an external electric field or bias voltage. Thus, our theoretical study will provide useful information whether the spin switching is achievable for potential spintronics purpose. Note that the external charge carrier is introduced in the same way as used in delta doped (Ga,Mn)As[29].

6.1.2. Numerical Method

In this report, our primarily interest is to explore whether it is possible to control the magnetic interaction between two magnetic layers by changing the external carrier type or the carrier concentrations in face centered cubic Co(111)/Gr/Ni(111) system. To this end, it is necessary to obtain magnetic ground state when there is no external carries. The thin film version of full potential linearized augmented plane (FLAPW) method for magnetic properties is used. Therefore, no shape approximation is assumed in charge, potential, and wavefunction expansions [43-45]. We treat the core electrons fully

relativistically, and the spin orbit interaction among valence electrons is dealt with second variationally [86]. The generalized gradient approximation is employed to describe exchange and correlation potentials [87]. Spherical harmonics with lmax = 8 are used to expand the charge, potential, and wavefunctions in the muffin-tin region. Energy cut offs of 16 Ry and 289 Ry are implemented for the plane wave star function and basis expansions in the interstitial region. It is assumed that the Co/Gr/Ni can be grown pseudomorphically, thus the lattice constant of 4.65 atomic unit × 4.65 atomic unit in lateral direction is employed. The muffin-tin radius of 2.2, 2.2, and 1.3 atomic unit is used for Ni, Co, and carbon, respectively. The structure optimization has been performed through force and energy minimization procedure. The entire calculations have been performed with 584 k-points.

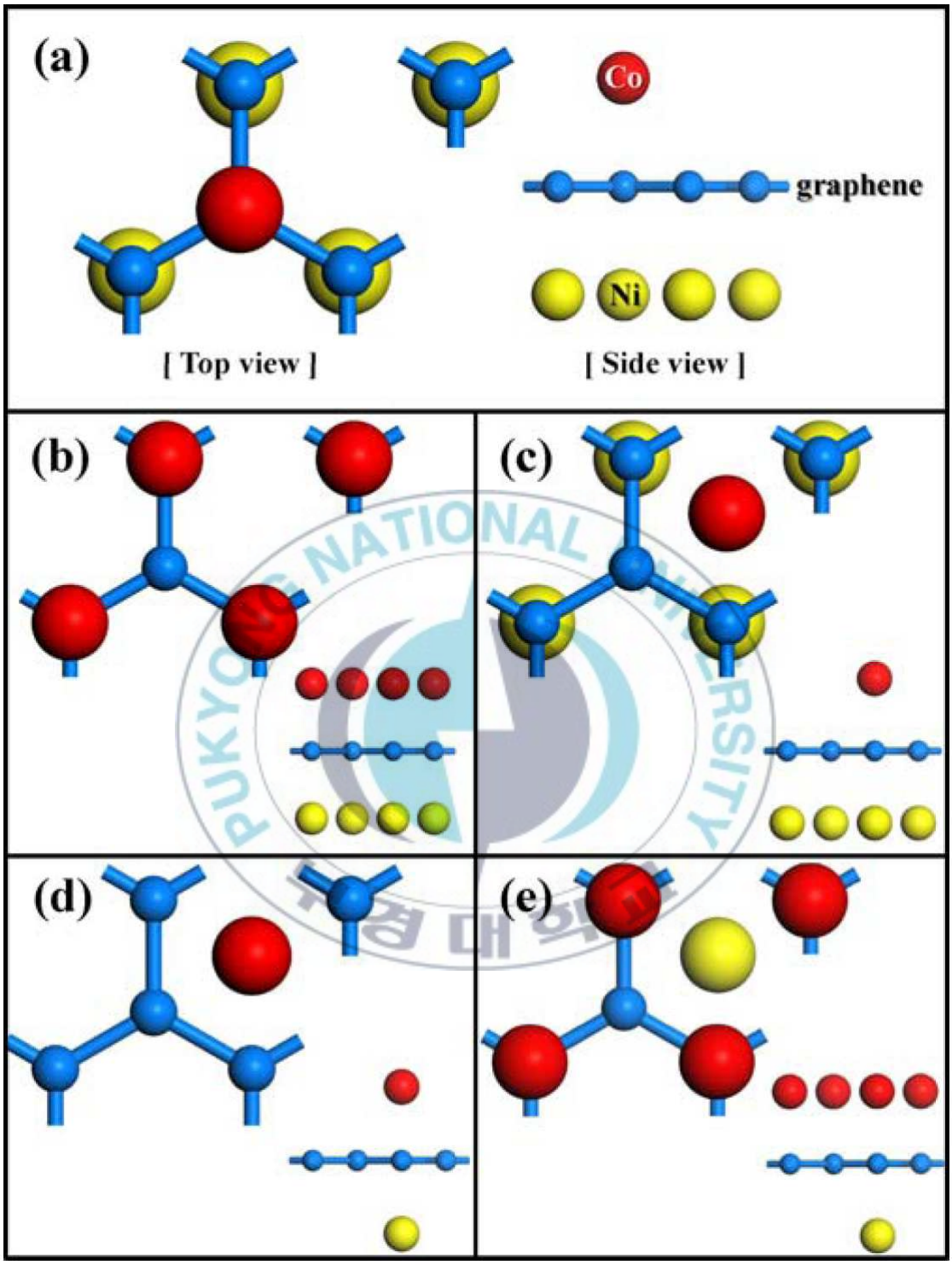

Figure 12. Top view of five possible adsorption structure of Ni/Gr/Ni system. The inset displays side view. The blue balls denote carbon atoms and the yellow ones are for Ni atoms.

6.1.3. Result and discussion

In Fig. 12, the five possible adsorption structures are presented. The blue, red, and yellow balls stand for graphene, Co, and Ni layers, respectively.

	FM	AFM	NM
Type I	not seen	−87 (−0.22, 1.50)	0
Type II	not seen	84 (−0.50, 1.82)	237
Type III	180 (0.51, 1.90)	not seen	401
Type IV	58	59	696
Type V	54	69	310

Table 3. Total energy (in meV/cell) and magnetic moment (in μ_B) in muffin-tin region (in parenthesis).

In Table 3, we present the calculated total energies and magnetic moments. The total energy of the non-magnetic (NM) state in type I structure is set to zero as a reference. We find that the magnetic state depends on the adsorption structure, but the most stable structure is realized in the type I configuration and the AFM ground state is achieved. In this ground state, the calculated magnetic moment of Ni is $-0.22\mu_B$, while the Co layer has $1.50\mu_B$. Note that the relative spin direction becomes antiparallel each other after self-consistent iterations even if we start the calculation with the FM configuration. The optimized structure is presented in Fig. 13(a). The distance between

carbon and Co is 2.07 Å and that between carbon and Ni is 2.04 Å. The relative height difference between two carbon atoms in graphene layer is 0.29 Å. To understand the effect of buckling geometry, we have performed the calculations without any buckling factor like in Fig. 13(b). In this case, the calculated magnetic moments of Ni and Co are $-0.60\ \mu_B$ and $1.70\mu_B$, respectively. From these results, one can see that the spin magnetic moments of Ni and Co are suppressed due to the strong bonding. Nonetheless, the magnetic ground state is insensitive to the strcuture optimization. This implies that AFM coupling is an intrinsic property of the Co/Gr/Ni system.

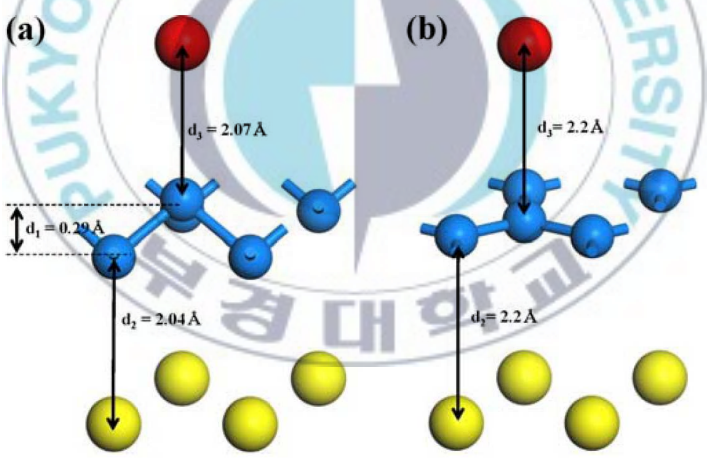

Figure 13. (a) Relative distances after structure optimization (b) ideally flat Co/Gr/Ni without any buckling feature.

The main issue is to study the influence of an external carrier on the magnetic property. Very recently, Efetov and Kim have reported that the graphene system could maintain ultra high carrier concentration

(about 10^{14} per cm^2 for both electrons or holes) [75]. Based on this experimental observation, we also used the same order of carrier concentrations in our calculations. The total energy differences according to the carrier types and concentrations are shown in Fig. 14. For hole carriers, there is found no FM state and the energy differences between the AFM and the PM states are presented by blue circles. The hole carriers do not affect the magnetic ground state since the AFM interaction between the Co and the Ni layer is still observed until the carrier density reaches approximately 2×10^{14} per cm^2. For electron carriers, very surprisingly, a potential switching from AFM to FM is observed if the carrier density reaches a certain critical value. For instance, the AFM state is still found at roughly 1×10^{13} per cm^2. Beyond this critical concentration, the FM phase appears (red circles). Note that we do not see any AFM state even if we start the calculation with AFM configuration.

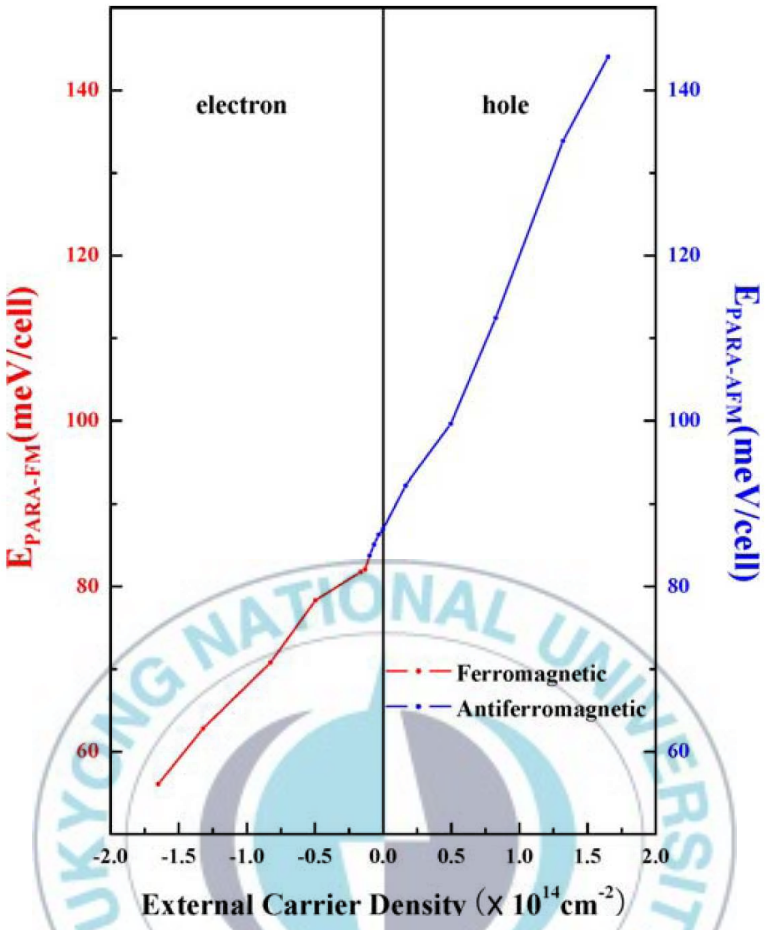

Figure 14. Total energy differences according to the carrier type and carrier concentrations.

In Fig. 15, the calculated density of states (DOS) of Ni, Co, and graphene layers are shown for various carrier concentration. Here, we just present the DOS with normal (no external carriers) and electron carriers at concentrations of 1.65×10^{14} per cm^2. For hole carriers, the DOS of Co and Ni layers is rigidly shifted with respect to the Fermi level as the concentration changes and no significant changes have been observed. Thus, the antiparallel coupling between Ni and Co is

still preserved. For electron carriers, the magnetic state of Co is rather robust since there is no significant modification. In contrast, the DOS of Ni layer is substantially altered when the electron carriers exist. The substantial changes occur in $|m|=0$ and $|m|=2$ orbitals, whereas the $|m|=1$ orbitals (or d_{xy}, d_{yz}) do not play an role for the switching of magnetic interaction. In particular, one can clearly see that the most dramatic change takes place in-plane states ($d_{x^2-y^2}, d_{xy}$, or $|m|=2$). These orbitals are negatively spin polarized in normal state, but the reversed spin polarization is achieved due to electron carriers. Of course, the similar behavior is observed in out-of-plane orbital ($d_{r^2-z^2}$, or $|m|=0$), but it is rather weak. Consequently, the carrier induced switching of magnetic interaction stems from the change of magnetic state Ni layer. It is found that the DOS of graphene layer at the Fermi level is almost negligible, but the pz state is seen in the presence of electron carriers. This may indicate that the Ruderman-Kittel-Kasuya-Yosida (RKKY) type interaction mediated by garphene layer plays a role for the switching from AFM to FM. However, to clearly understand the mechanism, it is necessary to investigate the systems in detail, for instance change the thickness of graphene layer or the type of 3d metal layers. This will be studied in the near future.

On the other hand, in the presence of external carriers, we attribute the FM coupling to the 2p-3d interaction and this can be understood from the DOS behavior. Although we have not directly calculated the

spin dependent transport properties, the calculated DOS provides other interesting behaviors.

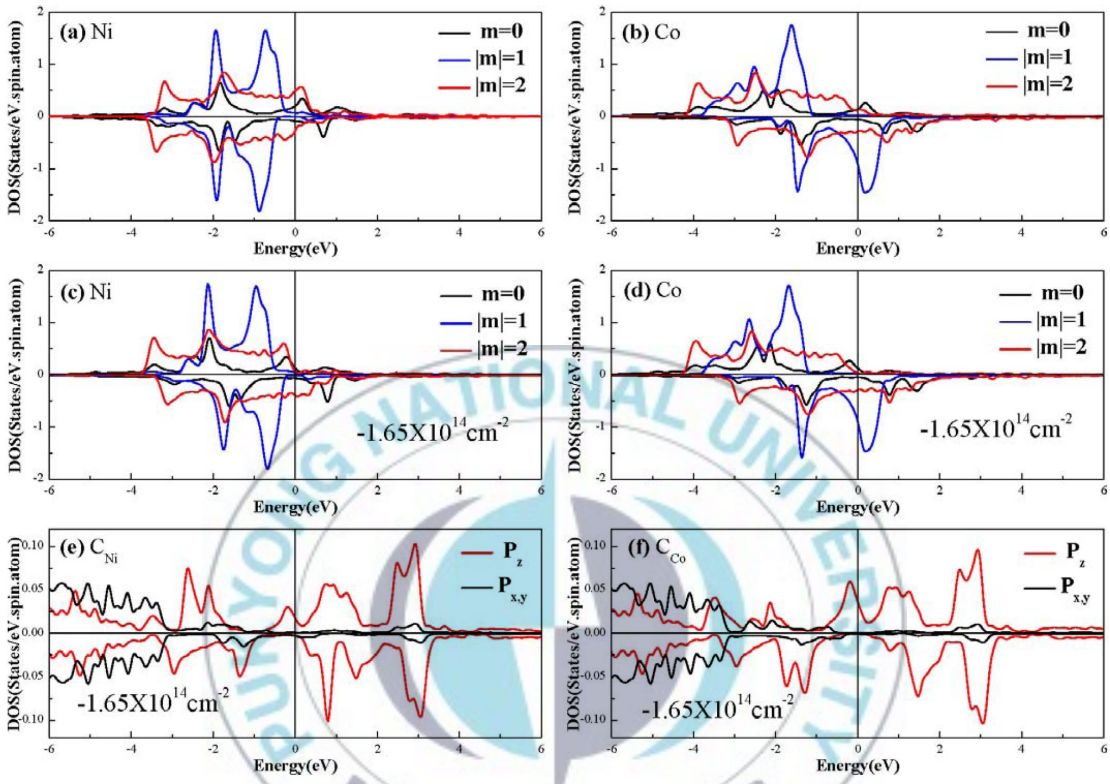

Figure 15. m-resolved DOS of (a) Ni atom without external carriers (b) Co atom without external carriers (c) Ni atom with electron carriers (d) Co atom with electron carriers (e) carbon atom hybridized with Ni (f) carbon atom hybridized with Co.

If the band structure is not substantially altered by a small external bias, the $|m|=2$ orbitals will contribute to the current which is parallel to the film surface and the majority spin states of Ni and Co are almost zero at the Fermi level. Thus, the parallel current will be completely spin polarized due to half metallic character. Note that there is no available parallel component of DOS from graphene layer.

As a result, the current will flow only through Co and Ni layers and the negatively spin polarized current is achievable in this direction. In addition, the minority spin DOS of graphene layer in p_z state will be completely suppressed, thus the majority spin electrons will move from Co to Ni layer or vice versa if the bias voltage is applied along the perpendicular direction to the film surface. Therefore, the completely spin polarized current can also be generated, but the current will be positively spin polarized, whereas it is negatively spin polarized along the parallel direction. A similar behavior is seen when the electrons move from the Ni to the Co layer.

6.1.4. Summary

In conclusion, we have investigated the potential carrier-induced switching of the magnetic interaction in Co/Gr/Ni systems. The Co/Gr/Ni is found to have an AFM state when there are no external carriers. The AFM ground state is still preserved even in the presence of hole carriers. However, we report that manipulation of the exchange coupling between two magnetic layers are probably achievable by injecting a certain amount of external electron carriers. Here, the carrier-induced spin switching from AFM to FM stems from the Ni layer because the magnetic state of the Ni layer changes according to the carrier type. The peculiar feature of the DOS imply that it is feasible to a generate highly spin polarized current from minority spin

electrons in a direction parallel to the film surface. In contrast, a completely spin polarized current from majority spin electrons will be obtained along the perpendicular to the film surface. Overall, we propose that the Co/graphene/Ni system may be a good candidate for spin switching purpose by applying external bias.

7. Conclusion and Discussion

We have investigate the magnetism of boron nitride or graphene systems using the full potential lineaized augmented plane wave (FLAPW) method.

It has been observed that the N vacancy defect has no influence on the magnetic property of h-BN, whereas the B vacancy defect caused spin polarization in the nearest three N atoms. The total magnetic moment is about $0.87\mu_B$ within muffin-tin radius (0.29 μ_B per N atom) and the spin polarized N atoms show metallic feature. In the presence of B adatom defect, we have obtained rather weak spin polarization about $0.1\mu_B$. However, the sizable magnetic moment of 0.38 μ_B appears in N adatom defect. Both B and N adatom defect systems preserve very close to semiconducting feature with a finite band gap. We have found that the DOS and the XMCD spectral shapes are strongly dependent on the defect type existing in the h-BN monolayer and this finding may help reveal the origin of magnetism in the h-BN layer if one performs surface sensitive experiment such as spin polarized scanning tunneling microscopy or XMCD measurement in the near future.

Also, we have investigated the magnetic properties of a hexagonal

boron nitride (h-BN) monolayer induced by a 0.5 monolayer of oxygen (O) and fluorine (F). It has been observed that the F and O adlayers are adsorbed on the boron top site in the most stable structure. We find that both systems display ferromagnetic ground states. In F/BN, the calculated magnetic moments of F and N atoms are 0.18 and $0.44\ \mu_B$, respectively. Also, the band structure of F/BN is very close to half-metallic. In O/BN, the calculated magnetic moments of O and N atoms are 0.91 and $0.4\mu_B$, respectively. The calculated band structure shows a metallic state. In addition, the calculated x-ray absorption spectroscopy and x-ray magnetic circular dichroism are presented.

Finally, we report the theoretical results that the carrier induced switching of magnetic interaction between two magnetic layers in Co(111)/Graphene/Ni(111) (Co/Gr/Ni) is predicted. The Co/Gr/Ni shows an antiferromagnetic (AFM) ground state when there are no external carriers. The antiferromagnetic interaction is still observed for hole carriers. Very interestingly, however, the magnetic exchange interaction between Ni and Co layers can be manipulated in such a way as to change an AFM to a ferromagnetic (FM) state by injecting external electrons if the electron carrier concentration is larger than 0.1×10^{14} per cm^2. Overall, we propose that a potential spin switching by external carriers or electric field can be realized in Co/Gr/Ni. Besides, the calculated DOS feature indicates that the Co/Gr/Ni system may manifest quite different transport properties when a bias voltage is

applied. For instance, the current parallel to the film surface can be completely spin polarized from minority spin electrons. In contrast, the current perpendicular to the film surface will be positively spin polarized from majority spin electrons.

8. Reference

[1] M. Venkatesan, C. B. Fitzgerald and J. M. D. Coey, Nature 430, 630 (2004).

[2] A. H. Castro Neto, F. Guinea, N. M. R. Peres, K. S. Novoselov, A. K. Geim, Condensed Matter arXiv:0709.1163 7 Sep (2007).

[3] Phillips, P. , Annals of Physics 321, 1634 (2006)

[4] Castro Neto, A. H., F.Guinea, and N.M.R. Peres, 2006a, Physics World 19, 33

[5] J. Yang, D. Kim, J. Hong and X. Qian, Surf. Sci. 604, 1603 (2010).

[6] D. Kim, J. Yang and J. Hong, J. Phys. Condens. Matter 22, 486006 (2010).

[7] P. O. Lehtinen, A. S. Foster, Y. Ma, A. V. Krasheninnikov and R. M. Nieminen, Phys. Rev. Lett. 93, 187202 (2004).

[8] M. Ventatesan, C. B. Fitzerald and J. M. D. Coey, Nature 430, 630 (2004).

[9] O. Rader, A. Varykhalov, J. Sanchez-Barriga, D. Marchenko, A. Rybkin and A. M. Shikin, Phys. Rev. Lett. 102, 057602 (2009).

[10] Y. S. Dedkov, M. Fonin, U. Rudiger and C. Laubschat, Phys. Rev. Lett. 100, 107602 (2008).

[11] M. I. Katsnelson, K. S. Novoseliv and K. Geim, Nature 2, 620 (2006).

[12] A. Varykhalov, J. Sanchez-Barriga, A. M. Shikin, C.Biswas, E.

Vescovo, A. Rybkin, D. Marchenko and O.Rader, Phys. Rev. Lett. 101, 157601 (2008).

[13] Q. Yu, J. Lian, S. Siriponglert, H. Li, Y. P. Chen and S.Pei, Appl. Phys. Lett. 93, 113103 (2008).

[14]L. H. Tomas, Proc. Camb. Phil. Soc. 23. 542(1926)

[15] E. Fermi, Z, Phys. 48,73 (1928).

[16] P. A. M. Dirac, Proc. Camb. Phil. Soc. 26, 376 (1930).

[17] P. Hohenberg and W. Kohn, Phys. Rev. 136, B 864 (1964).

[18] W. Kohn and L. J. Sham, Phys. Rev. 140, A1133 (1965).

[19] L. Hedin and S.J.Lundqvist , Phys. (France) 33, C3-73 (1972).

[20] J. von Barth and L. Hedin, J. Phys. C 5, 1629 (1972).

[21] O. Gunnarsson, B. I. Lundqvist, and Lundqvist, Solid State Commun. 11 149 (1972).

[22] A. D. Becke, Phys. Rev. A 38, 3098 (1988).

[23] J. P. Perdew and Y. Wang, Phys. Rev. B 45, 13244 (1992).

[24] M. Weinert, E. Wimmer, and A.J.Freeman, Phys. Rev. B 26, 4571 (1982).

[25] 홍순철, 이재일, “표면, 계면, 박막 자성에 대한 전자 구조 이론”, 한국자기학회지 Vol 5, No 4, 315 (1995).

[26] R. Asahi, Ph.D. Northwestern University, Evanston, Illinois, (1999)

[27] M. Weinert, R. E. Watson and J. W. Davenport, Phys. Rev. B 32, 2115 (1985).

[28] D. S. Wang, R. Wu and A. J. Freeman, Phys. Rev. Lett., 70, 869

(1993)

[29] X. D. Wang, R. Wu, D. S. Wang and A. J. Freeman, Phys. Rev. B 54, 61 (1996)

[30] A. H. MacDonald, W. E. Pickett and D. D. Koelling, J. Phys. C, 2675 (1980).

[31] A. Nagashima, N. Tejima, Y. Gamou, T. Kawai, C. Oshima, Phys. Rev. Lett. 75 3918 (1995)

[32] N.G. Chopra, R.J. Luyken, K. Cherry, V.H. Crepsi, M.L. Cohen, S.G. Louie, A. Zettl, A. Nagashima, N. Tejima, Y. Gamou, T. Kawai, C. Oshima, Science 269 966(1995)

[33] L. Bourgeois, Y. Bando, W.Q. Han, T. Sato, Phys. Rev. B 61 7686 (2000)

[34] D. Pacile, J.C. Meyer, C.O. Girit, A. Zettle, Appl. Phys. Lett. 92 133107 (2008)

[35] D. Golberg, Y. Bando, C. Tang, C. Zhi, Adv. Mater. 19 2413 (2007)

[36] M. S. Si, D.S. Xue, Phys. Rev. B. 75 193409(2007)

[37] M. Topsakal, E. Akturk, S. Ciraci, Phys. Rev. B 79 115442 (2009)

[38] V. Barone, J.E. Peralta, Nano Lett. 8 2210 (2008)

[39] Ru-Fen Liu, Ching Cheng, Phys. Rev. B 76 014405 (2007)

[40] R. Q. Wu, L. Liu, G.W. Peng, Y.P. Feng, Appl. Phys. Lett. 86 122510 (2005)

[41] S. Azevedo, J.R. Kaschny, C.M.C. de Castilho, F. de Brito Mota, Eur. Phys. J. B. 67. 507 (2009)

[42] F. Li, Z. Zhu, X. Yao, G. Lu, M. Zhao, Y. Xia, Y. Chen, Appl. Phys. Lett. 92 102512 (2008)

[43] E. Wimmer, H. Krakauer, M. Weinert, A.J. Freeman, Phys. Rev. B 24 864 (1981)

[44] M. Weinert, E. Wimmer, A.J. Freeman, Phys. Rev. B 26 4571 (1982)

[45] M. Weinert, J. Math. Phys. 22 2433 (1981)

[46] D. D. Koelling, B.N. Hamon, J. Phys. C: Solid State Phys. 10 3107 (1997)

[47] J. P. Perdew, K. Burke, M. Ernzerhof, Phys. Rev. Lett. 77 3865 (1996)

[48] M. J. Gillan, J. Phys. Condens. Mater 1 689 (1989)

[49] Doniach, M. Sunjic, J. Phys. C 3 285 (1970)

[50] M. Venkatesan, C. B. Fitzgerald and J. M. D. Coey Nature 430 630 (2004)

[50] D. Kim, J. Yang and J. Hong : J. Phys.: Condens. Matter22 486006 (2010)

[52] N. H. Hong, J. Sakai , N. Poirot and V. Brize Phys. Rev. B73 132404 (2006)

[53] I. S. Elfimov, S. Yunoki and G. A. Sawatzky Phys. Rev. Lett.89 216403 (2002)

[54] E. V. Castro , N. M. R. Peres, T. Stauber and N. A. P. Silva Phys. Rev. Lett. 100 186803 (2008)

[55] H. Ohldag,T. Tyliszczak,R. Hohne, D. Spemann, P. Esuqinazi ,M. Ungureanu and T. Butz Phys. Rev. Lett. 98 187204(2007)

[56] T. L. Makarova and F. Palacion (ed) Carbon Based Magnetism (Amsterdam: Elsevier) (2006)

[57] A. Nagashima, N. Tejima, Y. Gamou, T. Kawai and C. Oshima Phys. Rev. Lett. 75 3918

[58] N. G. Chopra et al Science 269 966 (1995)

[59] M. S. Si and D. S. Xue Phys. Rev. B 75 193409 (2007)

[60] M. Topsakal, E. Akturk and S. Ciraci Phys. Rev. B79 115442 (2009)

[61] V. Barone and J. E. Peralta Nano Lett. 8 2210 (2008)

[62] J. Yang, D. Kim, J. Hong and X. Qian Surf. Sci. 604 1603 (2010)

[63] J. Zhou, Q. Wang, Q. Sun and P. Jena Phys. Rev. B81 085442 (2010)

[64] S. Doniach and M. Sunjic J. Phys. C 3 285 (1970)

[65] Rep. Prog. Phys. 59 (1996) 1409–-1458. Printed in the UK

[66] O. K. Andersen, Linear methods in band theory, Phys. Rev. B 12, 3060 (1975).

[67] A. R. Williams, J. K¨ubler, and C. D. Gelatt Jr., Cohesive properties of metallic compounds: Augmented-Spherical-Wave calculations, Phys. Rev. B 19, 6094 (1979).

[68] Computational Nanoscience Vol. 31, ISBN 3-00-017350-1, pp. 85-129, 2006.Stefan Bl ¨ugel and Gustav Bihlmayer

[69] K. S. Novoselov, A. K. Geim, S. V. Morozov, D. Jiang, Y. Zhang, S. V. Dubonos, I. V. Grigorieva and A. A. Firsov, Science 306, 666 (2004).

[70] Y. Zhang, Y. W. Tan, H. L. Stromer and P. Kim, Nature 438, 201 (2005).

[71] M. Fuentes-Cabrera, M. I. Baskes, A. V. Melechko and M. L. Simpson, Phys. Rev. B 77, 035405 (2008).

[72] J. Yang, D. Kim, J. Hong and X. Qian, Surf. Sci. 604, 1603 (2010).

[73] D. Kim, J. Yang and J. Hong, J. Phys. Condens. Matter 22, 486006 (2010).

[74] P. O. Lehtinen, A. S. Foster, Y. Ma, A. V. Krasheninnikov and R. M. Nieminen, Phys. Rev. Lett. 93, 187202 (2004).

[75] M. Ventatesan, C. B. Fitzerald and J. M. D. Coey, Nature 430, 630 (2004).

[76] O. Rader, A. Varykhalov, J. Sanchez-Barriga, D. Marchenko, A. Rybkin and A. M. Shikin, Phys. Rev. Lett. 102, 057602 (2009).

[77] Y. S. Dedkov, M. Fonin, U. Rudiger and C. Laubschat, Phys. Rev. Lett. 100, 107602 (2008).

[78] M. I. Katsnelson, K. S. Novoseliv and K. Geim, Nature 2, 620 (2006).

[79] A. Varykhalov, J. Sanchez-Barriga, A. M. Shikin, C.Biswas, E. Vescovo, A. Rybkin, D. Marchenko and O.Rader, Phys. Rev. Lett. 101,

157601 (2008).

[80] Q. Yu, J. Lian, S. Siriponglert, H. Li, Y. P. Chen and S.Pei, Appl. Phys. Lett. 93, 113103 (2008).

[81] Y. Ohno, D. K. Young, B. Beschoten, F. Matsukura, H.Ohno and D. D. Awschalom, Nature 402, 790 (1999).

[82] H. Ohno, D. Chiba, F. Matsukura, T. Omiya, E. Abe, T.Dietl, Y. Ohno and K. Ohtani, Nature 408, 944 (2000).

[83]D. Chiba, M. Yamanouchi, F. Matsukura and H. Ohno,Science 301, 943 (2003).

[84] J. Hong, D. S. Wang and R. Q. Wu, Phys. Rev. Lett. 94,137206 (2005).

[85] V. M. Karpan, G. Giovannetti, P. A. Khomyakov, M. Talanana,A. A. Starikov, M. Zwierzycki, J. van den Brink,G. Brocks and P. J. Kelly, Phys. Rev. Lett. 99, 176602 (2007).

[86] D. D. Koelling and B. N. Hamon, J. Phys. C: Solid State Phys. 10, 3107 (1997).

[87] J. P. Perdew, K. Burke and M. Ernzerhof, Phys. Rev.Lett. 77, 3865 (1996).

[88] D. K. Efetov and P. Kim, Phys. Rev. Lett. 105, 256805(2010).

[89] The Korringa-Kohn-Rostoker (KKR) Green Function Method by Ph. Mavropoulos on page 131

9. Publications

1. Dongyoo Kim, Jeonghwa Yang and Jisang Hong, "Carrier-induced Spin Swiching in Co/Graphene/Ni: A First principles Study" Journal of the Korean Physical Society, 60,420 (2012)

2. Dongyoo Kim, Jeonghwa Yang and Jisang Hong, "Ag-induced large perpendicular magnetic anisotropy in Mn/Ag/Fe(001)" Journal of Applied Physics, 110, 083924 (2011)

3. Jeonghwa Yang, Dongyoo Kim and Jisang Hong, "Potential Room Temperature Ferromagnetic O/BN and F/BN Bilayers" Journal of Physics: Condensed Matter, 23, 066001 (2011)

4. Jeonghwa Yang, Dongyoo Kim and Jisang Hong " Magnetism in Boron nitride monolayer: Adatom and Vacancy defec" Surface Science,604, 1603 (2010)

5. Dongyoo Kim, Jeonghwa Yang and Jisang Hong "Mg Vacancy Defect Induced Half Metallic MgO(001) Film" Journal of the Korean Physical Society, 56, L1729 (2010)

6. Dongyoo Kim, Jeonghwa Yang and Jisang Hong " Magnetic Property of Carbon Doped ZnO and X-ray Magnetic Circular Dichroism: A First

Principles Study" Journal of the Korean Physical Society, 56,1446 (2010)

7. Dongyoo Kim, Jeonghwa Yang and Jisang Hong "Magnetic anisotropy and Magneto Optical Property of Fe/Co/Cu(001): Role of The Interface Alloy" Journal of the Korean Physical Society, 56, 78 (2010)

8. Dongyoo Kim, Jeonghwa Yang and Jisang Hong " Large Perpendicular Magnetic Anisotropy of Ultrathin Ru and Rh Films on A NiAl(001) Surface" Journal of Physics: Condensed Matter, 22, 426003 (2010)

9. Dongyoo Kim, Jeonghwa Yang and Jisang Hong "Ultrathin Half Metallic N and Antiferromagnetic Semiconduction C layers on MgO(001)" Journal of Physics: Condensed Matter, 22, 486006(2010)

10. Dongyoo Kim, Jeonghwa Yang and Jisang Hong "Giant Perpendicular Magnetic Anisotropy of An Ir Monolayer on A NiAl(001) Surface" Physical Review B, 80, 052404(2009)

11. Dongyoo Kim, Jeonghwa Yang and Jisang Hong "Magnetic Anisotropy and Magneto-Optical Kerr Effect of BCC Ni(001) Films:Ab-initio Study" Journal of the Korean Physical Society, 55, 2537 (2009)

12. Dongyoo Kim, Jeonghwa Yang and Jisang Hong "Manipulation of Spin Reorientation Transition by Au Capping in Body-Centered Cubic Ni(001) film" Journal of Physics: Condensed Matter, 20, 485010 (2008)